

FRACTIONAL FOURIER TRANSFORM BASED BRAIN COMPUTER
INTERFACE SYSTEM FOR PERSON AUTHENTICATION



MCS

By

Intisar Rizwan-i-Haque

Thesis submitted to the Faculty of the Department of Electrical Engineering, College of
Telecommunications (MCS), National University of Sciences and Technology, Pakistan
in partial fulfillment for the requirements of MS degree in Electrical
(Telecommunication) Engineering

July, 2012

IT WOULD BE POSSIBLE TO DESCRIBE EVERYTHING
SCIENTIFICALLY, BUT IT WOULD MAKE NO SENSE; IT
WOULD BE WITHOUT MEANING, AS IF YOU
DESCRIBED A BEETHOVEN SYMPHONY AS A
VARIATION OF WAVE PRESSURE.

Albert Einstein

ABSTRACT

A Biometric system utilizes biological characteristics like DNA, Voice, Ear, Face, Finger prints to uniquely establish user identity. Brain Computer Interface (BCI) based Biometric system relies on unique neural structure and mental activity signals commonly known as Electroencephalogram (EEG) signals to authenticate the user and are inherently immune to impersonation.

Details learned from existing applications of Fractional Fourier Transform (FRFT) were used to devise an algorithm that utilized fractional coefficients extracted from subject specific EEG patterns for various tasks performed by the user. The advantage of using Fractional Fourier Transform is that it offers improved performance for systems that are based on Fourier Transform with little additional cost and as it's a linear one dimensional Time-Frequency distribution it is more suitable for time-varying EEG signals than Fourier Transform. Exact Radial Basis (RBE) Neural Network was used for classification due to its advantage of low training time. A special one dimensional case of k-means clustering was used to calculate the threshold in order to accept the user as a client or reject him as an imposter. The proposed system works on signals recorded from multiple channels, therefore Weight Adjustment was carried out for each electrode and task performed by the user.

The performance improvements as a result of weight adjustment and the efficiency of the proposed algorithm were tested on pre-recorded dataset available from Colorado University and another dataset was self-recorded using the indigenously designed hardware prototype. The average accuracy achieved for both the datasets was more than 75% with response time of less than two seconds.

DEDICATION

“If Allah helps you none shall prevail over you; if He forsakes you then who can help you? It is in Allah that the believers should put their trust” (3:160)

Dedicated to my beloved family and to our country Pakistan

ACKNOWLEDGEMENT

This dissertation would not have been possible without the kind support and valuable assistance of several individuals who in one way or another contributed in the preparation and completion of this study.

First and foremost, my utmost debt of gratitude is to my Supervisor Maj. Dr. Naveed Iqbal Rao for his encouragement, guidance and continuous support throughout the research work.

I am also grateful to Lt. Col. Dr. Imran Touqeer and Dr. Saeed Murtaza for sparing their valuable time to provide input for the various mathematical equations used in this work.

I would also like to thank Curtis Condon, Ken White, and Al Feng of the Beckman Center at the University of Illinois for the bat data and for permission to use it in this work.

I would also like to acknowledge Anderson, C.W. and Kirby, M., of CSU EEG Brain Computer Interface Lab at the Colorado State University for the recorded EEG data and for permission to use it in this work.

Last but not the least, THE ALLAH ALMIGHTY, for answering my prayers and providing me the strength to tread on despite many difficulties, thank you so much Dear Lord.

Table of Contents

INTRODUCTION.....	1
1.1 Background.....	1
1.2 Statement of Problem.....	2
1.3 Objective.....	3
1.4 Research Methodologies and Goals.....	3
1.5 Scope of the Research.....	3
1.6 Document Organization.....	4
LITERATURE REVIEW	5
2.1 Introduction.....	5
2.2 Chirp Signal and Fourier Transform.....	5
2.3 Fractional Fourier Transform.....	9
2.4 Fractional Fourier Transform Numerical Computation.....	13
2.5 Wigner Distribution.....	14
2.6.1 Biometric System.....	16
2.6.2 Brain Computer Interface Composition.....	17
2.7 Summary.....	18
FRACTIONAL FOURIER TRANSFORM APPLICATIONS	19
3.1 Introduction.....	19
3.2 Filtering in Fractional Fourier Domain.....	19
3.3 Dimensional Normalization.....	23
3.3.1 Discrete Scaling Method (DSM):.....	23
3.3.2 Data Zero Padding/Interception Method (DZPIM):.....	24
3.4 Chirp Signal Parameter Estimation and Optimum Order.....	25
3.5 Maximum Amplitude Method for Compact FRFT Domain (MACF).....	31
3.6 FRFT for Biomedical Signal Detection.....	34
3.7 Summary.....	37
EXPERIMENTAL SETUP AND ALGORITHM DESIGN FOR PERSON AUTHENTICATION	38
4.1 Introduction.....	38
4.2 Data Acquisition.....	38
4.2.1 EEG Signal Acquisition Device.....	38

4.2.2	Self-Recorded Dataset – I and II.....	41
4.2.3	Pre-Recorded Colorado University Dataset.....	43
4.3	Pre-Processing.....	44
4.3.1	Colorado University Dataset.....	44
4.3.2	Self-Recorded Dataset – I and II.....	45
4.4	Feature Extraction.....	46
4.5	Classification.....	46
4.6	Network Weight Adjustment.....	48
4.6.1	Simple Majority Rule.....	48
4.6.2	Weight Adjustment.....	48
4.7	Performance Evaluation.....	51
4.8	Summary.....	51
RESULTS AND ANALYSIS		52
5.1	Introduction.....	52
5.2	Offline Pre-Recorded Dataset Results.....	52
5.3	Offline Self-Recorded Dataset-I Results.....	58
5.4	Offline Self-Recorded Dataset-II Results.....	61
5.5	Comparison Existing Techniques.....	66
5.6	Summary.....	67
CONCLUSION AND FUTURE WORK.....		68
6.1	Overview.....	68
6.2	Objectives Achieved.....	68
6.3	Future Work.....	68
6.4	Summary.....	69
BIBLIOGRAPHY.....		70

List of Figures

Figure No	Page No
2.1–Signal $\sin(t)$ and it's Fourier Transform.....	7
2.2–Signal ' $\sin(t) + \delta(t)$ ' and it's Fourier Transform	8
2.3–Signal $\sin(t^2)$ and it's Fourier Transform	9
2.4–Rotation of the signal by Fractional Angle α	10
2.5–FRFT of Rectangular Pulse for Orders 0, 0.2, 0.4, 0.6, 0.8 and 1	12
2.6–Rotation of Time-Freq. Representation of Chirp Signal	15
2.7–Block Diagram of typical BCI Based Biometric System	17
3.1–Filtering in Fractional Domain Example 1	20
3.2–Filtering in Fractional Domain Example 2	22
3.3–Effect of Dimensional Normalization (DSM) Example 1	28
3.4–Effect of Dimensional Normalization (DZPM) Example 2	30
3.5–Optimum Order for Signal emitted by Large Brown Bat.....	33
3.6–Biomedical Signal Detection in presence of AWGN noise	35
3.7–Biomedical Signal Detection of Multi-Component Chirp Signal	37
4.1–EEG Signal Acquisition Device	38
4.2–Second Order Multiple Feedback Low Pass Filter.....	40
4.3–Amplitude Spectrum of Composite Signal.....	41
4.4–EEG Signals Recording of 7 Electrodes.....	43
4.5–Demodulated Four Channel EEG Data	45
4.6–Order Optimization.....	46
4.7–Radial Basis Function Response for Spread = 1	47
5.1–Individual Electrode \overline{HTER} Performance Curve for Subj. 1	52
5.2–Individual Electrode \overline{HTER} Performance Curve for Subj. 3.....	53

5.3–Individual Electrode \overline{HTER} Performance Curve for Subj. 4.....	53
5.4–Individual Electrode \overline{HTER} Performance Curve for Subj. 6.....	54
5.5–Weight Adjusted Performance for each Mental Imagery task	58
5.6–Individual Electrode Performance for Subj. 2	59
5.7–Individual Electrode Performance for Subj. 3	59
5.8–Individual Electrode Performance for Subj. 1 Dataset - II.....	61
5.9–Individual Electrode Performance for Subj. 2 Dataset - II.....	61
5.10–Individual Electrode Performance for Subj. 3 Dataset - II.....	62
5.11–Individual Electrode Performance for Subj. 4 Dataset - II.....	62
5.12–Individual Electrode Performance for Subj. 5 Dataset - II.....	62
5.13–Individual Electrode Performance for Subj. 6 Dataset - II.....	63
5.14–Individual Electrode Performance for Subj. 7 Dataset - II.....	63
5.15–Individual Electrode Performance for Subj. 8 Dataset - II.....	63
5.16–Individual Electrode Performance for Subj. 9 Dataset - II.....	64
5.17–Individual Electrode Performance for Subj. 10 Dataset - II.....	64
5.18–Individual Electrode Performance for Subj. 11 Dataset - II.....	64

List of Tables

Table No	Page No
4.1–Individual Electrode Color Codes and Location	41
4.2–System Cues and Motor Imagery Tasks.....	42
4.3–Total Trials for Motor Imagery Tasks Dataset - I.....	42
4.4–Total Trials for Motor Imagery Tasks Dataset - II.....	42
5.1–Individual Electrode Accuracies	54
5.2–Optimum Orders for Mental Imagery Tasks Subject 1	55
5.3–Optimum Orders for Mental Imagery Tasks Subject 3	55
5.4–Optimum Orders for Mental Imagery Tasks Subject 4.....	55
5.5–Optimum Orders for Mental Imagery Tasks Subject 6.....	55
5.6–Weight Adjustment for Mental Imagery Tasks Subj. 1	56
5.7–Weight Adjustment for Mental Imagery Tasks Subj. 3	56
5.8–Weight Adjustment for Mental Imagery Tasks Subj. 4	56
5.9–Weight Adjustment for Mental Imagery Tasks Subj. 6	57
5.10–Expected System Performance for Mental Imagery Tasks	57
5.11–Individual Electrode Accuracies	60
5.12–Optimum Orders for Motor Imagery Tasks Subject 2	60
5.13–Optimum Orders for Motor Imagery Tasks Subject 3	60
5.14–Weight Adjustment for Motor Imagery Tasks Subj. 2.....	60
5.15–Weight Adjustment for Motor Imagery Tasks Subj. 3.....	60
5.16–Average Electrode Accuracies Dataset - II	65

INTRODUCTION

1.1 Background

Brain (Encephalon) is a complex vital structure of nerve cells more or less similar, which interact with each other to control all the functions of the human body by means of electrical activity commonly known as Electroencephalogram (EEG) signal. EEG signals can be recorded at the scalp by means of very high input impedance electrodes but are time-varying, inherently noisy with amplitude that is almost negligible, distorted by artifacts (eye blinks and muscular movement etc.) and are highly unpredictable in nature. The information retrieval or decoding of these signals by means of efficient signal processing techniques for smooth control of a machine or man-made devices is referred to as Brain Computer Interface (BCI). BCI offers one means of restoring communication for severely paralyzed people deprived of any motor functions, or patients in a “locked-in” syndrome [1].

A popular approach to implementing EEG based BCI system involves the use of Fourier Transform (FT) to extract features based on either energy or power spectral coefficients in different frequency bands. FT has a limitation that it represents any instantaneous changes in the signal by infinite number of frequencies with no information about the time location of the change that is poor time resolution. One solution to this problem is the use of Short Time Fourier Transform (STFT) that utilizes windowing function to analyze local sections of a signal for frequency content as it changes over time. The problem with STFT is that it has a fixed resolution and is dependent upon characteristics of windowing function like for example a wide windowing function gives better frequency resolution but poor time resolution and vice versa. To overcome the problem of fixed resolution is to use Wavelet Transform (WT) which is a multi-resolution technique but it provides for extremely poor results if Mother Wavelet does not closely represent the characteristics of the EEG signal.

Person authentication system involves one to one mapping of features of an individual claiming identity and either the individual will be accepted and referred to as a client or rejected as an imposter. Research in the field of BCI system indicates that EEG signals vary from one individual to another [30]. The underlying reason for the difference is the varying neural structure from one user to another. This leads to the possibility of usage of EEG signals for person authentication.

1.2 Statement of Problem

The performance of existing systems based on Fourier Transform can be further improved by the use of Fractional Fourier Transform (FRFT) as it provides the advantage of controlling the frequency & time content in the signal through fractional order. The Brain Computer Interface (BCI) via the FRFT results from the generalization of works carried out on Mental and Motor Imagery thought classification through the Fourier Transform (FT) [2], [3], given that the FT is a specific case of the FRFT, thus adding a new degree of freedom that improves the accuracy of the correct thought classification [4]. In my previous work as part of another team and reported in [4]; use of feature vectors made of Fractional Fourier coefficients as input to neural network for mental thought classification was proposed. The algorithm achieved an overall accuracy of correct thought classification $\approx 85\%$.

The problem with utilization of FRFT is that it is a relatively new area of research and as such has many computational algorithms and each with different implementation details. Another problem with FRFT is the question that what criterion defines the optimum order for a particular application and then how to find it. One of the approaches previously employed in BCI based control system was the use of exhaustive search which render the process of identifying the optimum order (defined as the order that provides the best system accuracy) to be quite slow.

EEG Signals in most BCI applications are acquired through multi-channel signal acquisition device. Existing approaches either concatenates the features extracted from each electrode into one feature vector or a parallel structure is employed and final classification decision is made on the basis of simple majority rule. In both of these approaches it is assumed that all the electrodes will exhibit same fidelity for various mental tasks which is usually not the case. Each electrode network

corresponds to a different region of the brain, and signals recorded from these locations vary for different subjects and tasks.

1.3 Objective

The main aim of research is to propose an algorithm and model capable of extracting such features from EEG signals that can authenticate a user with reasonable accuracy, low response time and computational complexity based on FRFT that will replace the existing FT based Feature Extractor. The algorithm will have lower computational complexity for order optimization than existing approaches based on exhaustive search. Also an automated approach to weight adjustment based on individual channel performance will be developed.

1.4 Research Methodologies and Goals

In order to achieve the desired objectives, the idea was to carryout review of existing literature and applications of Fractional Fourier Transform and to verify its implementation details through simulations in phase-1. On the basis of the information gained from the previous review, tests were run on the EEG signal database comprising multiple users and individual channel performances were obtained. Probabilities of correct classification for panel comprising the multiple channels with and without weight adjustment were carried out to predict the performance of the classifier and the proposed approach for various mental and motor imagery tasks.

1.5 Scope of the Research

The research work covers the analysis of a few existing applications of Fractional Fourier Transform and provides insight into their implementation details. The work culminated in development of an algorithm capable of optimizing the fractional orders and weight adjustment for EEG based person authentication. The initial tests run on multiple databases provided reasonable accuracy for a lower training data and response time compared to existing approaches.

1.6 Document Organization

Chapter 2 gives a review of Chirp Signal, Fourier Transform, Wigner Distribution, Fractional Fourier Transform and Brain Computer Interface. Chapter 3 discusses various applications of FRFT and provides insight into its implementation for a specific problem and lays out the basis for its utilization in an EEG based Biometric System. Chapter 4 provides comprehensive details of Algorithm and experimental setup. Chapter 5 details the results obtained from offline testing on recorded datasets. Chapter 6 concludes the research work and highlights the future work on the proposed system.

LITERATURE REVIEW

2.1 Introduction

This chapter starts with a basic review of Chirp Signals and Fourier Transform (FT). The various limitations of FT are pointed out and the Fractional Fourier Transform (FRFT) as a generalization of FT with some of its properties is introduced. The chapter ends with the details of Brain Computer Interface (BCI) for Electroencephalogram (EEG) based Person Authentication System.

2.2 Chirp Signal and Fourier Transform

Human Speech, Sound, Electromagnetic waves transmission through wired or wireless media and Biological potentials etc. are all examples of one dimensional signals represented in time. Plot of such signals will provide us information about the various trends present with in the signal like its peak amplitude, shape of the waveform (Sinusoid, Square or Ramp etc.) or when a particular spike occurs. An example of signal $x(t)$ expressed mathematically is given below:

$$x(t) = A\cos(\theta(t)) + W(t) \quad \dots (2.1)$$

Where A is the amplitude, $\theta(t)$ is the phase and $W(t)$ is the noise usually assumed to be Additive White Gaussian Noise (AWGN). Phase determines the type of the signal:

$$\theta(t) = \begin{cases} \text{constant} \\ (\omega_o t + \varphi) \\ (2\pi\mu_o t^2 + \omega_o t + \varphi) \end{cases} \quad \dots (2.2)$$

Here $\omega_o = \text{Angular Frequency} = 2\pi f_o t$ and f_o is known as either Fundamental or Initial or Central Frequency in literature. μ_o is known as Chirp Rate or Modulated Frequency Ratio and is defined as:

$$\mu_o = \frac{1}{2\pi} \frac{d^2\theta(t)}{dt^2} \quad \dots (2.3)$$

In general, Instantaneous Frequency (IF) is defined as:

$$IF = \frac{1}{2\pi} \frac{d\theta(t)}{dt} \quad \dots (2.4)$$

In Eq. (2.1), constant phase results in zero frequency (IF = 0, DC signal), linear phase results in constant frequency (IF = f_o , Sinusoid signal shown in Figure 2.1) and quadratic phase results in linearly increasing frequency with time (IF = $2\mu_o t + f_o$, Linear Frequency Modulation or Chirp signal shown in Figure 2.2). To create a chirp signal of duration T and a frequency change equal to $\Delta f = f_2 - f_1$, the equation of a line $y = mx + c$ can be used to obtain an equation for the instantaneous frequency:

$$f(t) = \frac{f_2 - f_1}{T} t + f_1 \quad \dots (2.5)$$

Fourier Transform (FT) of a signal provides the information about the spectral content of a signal. Mathematically,

$$X(e^{i\omega}) = \frac{1}{2\pi} \int_{-\infty}^{\infty} x(t) \cdot e^{-i\omega t} dt \quad \dots (2.6)$$

Transformation of $X(e^{i\omega})$ back to original signal i.e. the inverse Fourier Transform is given by:

$$X^{-1}(e^{i\omega}) = x(t) = \int_{-\infty}^{\infty} X(\omega) \cdot e^{i\omega t} dt \quad \dots (2.7)$$

In Eq. (2.6), 2π is the Transformation Factor (TF). TF in most applications in signal processing is distributed in both forward and backward transformations that is:

$$X(e^{i\omega}) = \frac{1}{\sqrt{2\pi}} \int_{-\infty}^{\infty} x(t) \cdot e^{-i\omega t} dt \quad \dots (2.8)$$

And

$$X^{-1}(e^{i\omega}) = x(t) = \frac{1}{\sqrt{2\pi}} \int_{-\infty}^{\infty} X(\omega) \cdot e^{i\omega t} dt \quad \dots (2.9)$$

For $\omega = 0$, Eq. (2.6) simply becomes area under a signal.

$$X(0) = \int_{-\infty}^{\infty} f(t) dt \quad \dots (2.10)$$

Fourier Transform of a signal $x(t)$ exists, if and only if the integral of $|x(t)|$ from $-\infty$ to ∞ exists and any discontinuities in $x(t)$ are finite. In case $x(t)$ is discontinuous the left hand side should be replaced by $\frac{1}{2}[x(t+) + x(t-)]$, that is by using unequal limits of $x(t)$ as t is approached from above and below. The waveforms like a sinusoidal signal $\sin(t)$ implies an AC signal which has to be switched on infinite time ago, Unit Step $u(t)$ means a signal switched on and maintained steady forever and the Impulse Function $\delta(t)$ has to be a signal that has to be infinitely large for an infinitely small time [5]. None of these signals are physically realizable in the strictest sense and their FT does not exist. But the approximations to these signals are used in almost all signal processing applications and therefore their FT is defined in the limiting sense. An AC sinusoidal signal $\sin(t)$ and its Fourier Transform are shown in Figure 2.1.

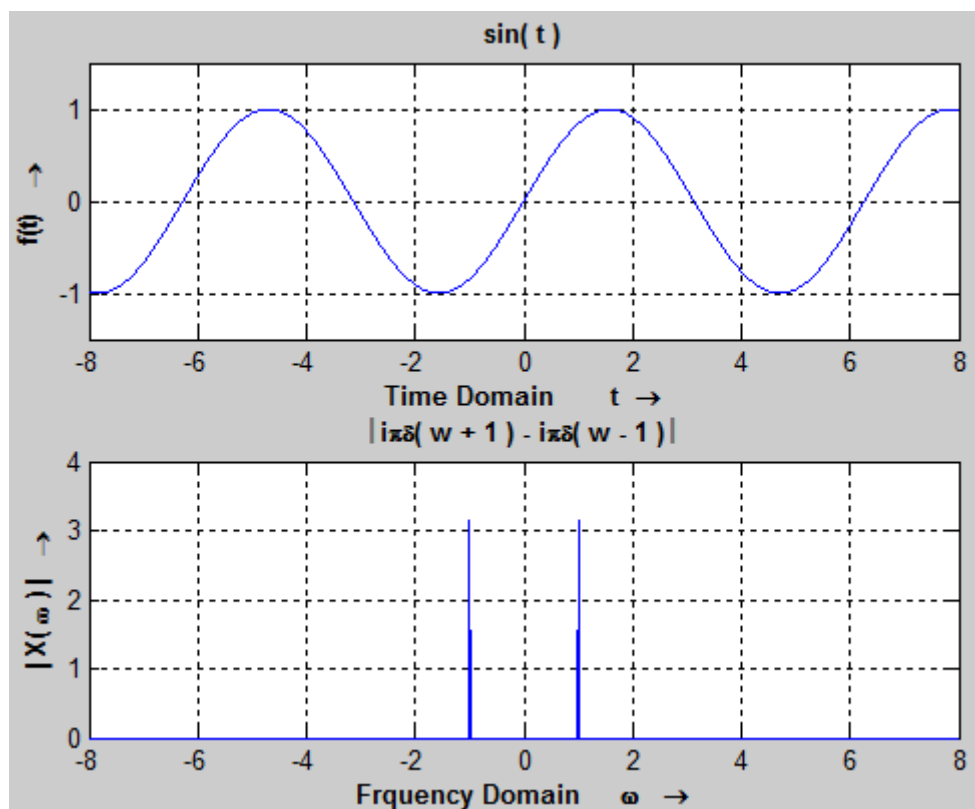


Figure 2.1–Signal $\sin(t)$ and its Fourier Transform

In Figure 2.1 the top portion displays time domain representation of signal $\sin(t)$. Fourier Transform of the signal results in an Impulse function with amplitude shown in the title of the frequency domain representation displayed in the bottom portion of

the Figure 2.1. As evident, Fourier Transform does not provide any information about time i.e., instantaneous changes in the signal. In order to elaborate the previous statement, a signal $\sin(t)$ distorted with an unit impulse occurring at time $t=0$ secs and its Fourier Transform representation is shown in Figure 2.2.

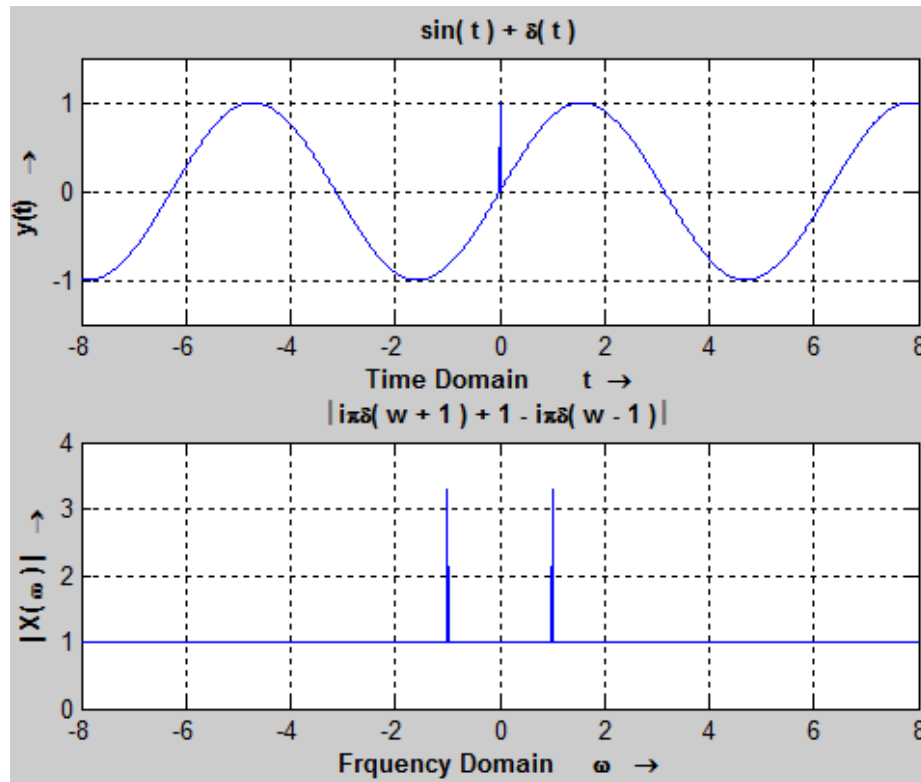


Figure 2.2–Signal ‘ $\sin(t) + \delta(t)$ ’ and it’s Fourier Transform

In Figure 2.2 the spike occurring in the signal at $t = 0$ sec is represented by infinite number of frequencies that does not provide any information about the location of the spike that is all information about time domain is lost as such it is impossible to tell when a particular event took place. On the other hand the signal itself provides information about the location of the spike but fails to provide any information about the various frequency components that are present in the signal.

Let’s consider a chirp signal $\sin(\omega t^2)$. Close inspection of the signal reveals that it can be written as $\sin(\omega t * t)$. Since $\sin(\omega t)$ contains a single frequency harmonic then $(\omega t * t)$ represents a linearly increasing frequency but FT returns a continuum of frequencies. A chirp signal $\sin(t^2)$ and its Fourier Transform representation is depicted in Figure 2.3.

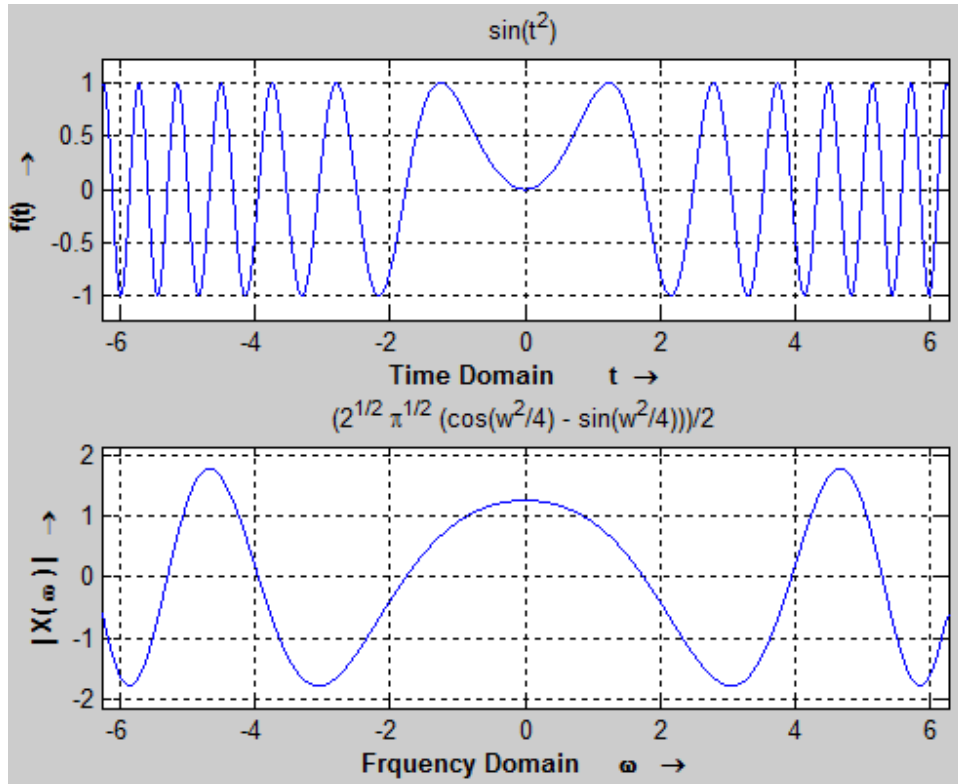


Figure 2.3–Signal $\sin(t^2)$ and it's Fourier Transform

In Figure 2.3 the top portion displays time domain representation of signal $\sin(t^2)$. Fourier Transform of the signal results in an another chirp function with amplitude shown in the title of the frequency domain representation displayed in the bottom portion of the Figure 2.3. This is because of the fact that conventional Fourier harmonic analysis views frequency and time as orthogonal variables and subsequently is only appropriate for the study of signals with stationary frequency content [6].

2.3 Fractional Fourier Transform

It is a common observation that FT applied twice to a signal returns flipped version of the original signal, applied thrice results in the flipped spectral contents and four times application returns the original signal back. This corresponds to the periodic nature of the Fourier operator and can be easily imagined by placing the time domain representation of the signal along x-axis and spectral content representation along y-axis in a two dimensional rectangular co-ordinate system as shown in Figure 2.4.

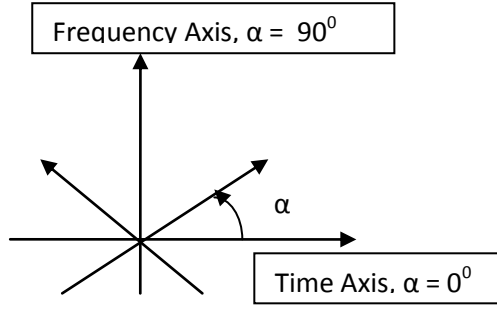


Figure 2.4–Rotation of the signal by Fractional Angle α

As evident, Fourier operator provides the signal representation along the axes only which raises an important question about what happens in between the axis. The answer lies in Fractional Fourier Transform (FRFT). Precisely as the Fourier analysis utilizes sinusoidal function to decompose periodic signals, Fractional Fourier techniques uses chirp harmonics for the time-varying periodicity signals decomposition [7]. It can be construed as the illustration of a signal in neutral domain by means of the rotation of the signal by the origin in counter-clockwise direction with rotational angle α in time-frequency domain [8], as shown in Figure 2.4, [4].

FRFT is a one dimensional time frequency distribution, with FT as a particular case. The FRFT of a signal $s(x_1)$ can be given as

$$F^p[s(x_1)] = S(x) = \int_{-\infty}^{\infty} K_p(x, x_1) s(x_1) d(x_1) \quad \dots (2.11)$$

Where $d(x_1)$ is the derivative with respect to x_1 and kernel function is defined by:

$$K_p(x, x_1) = C_\alpha e^{-i\pi(2\frac{x_1x}{\sin(\alpha)} - (x^2 + x_1^2) \cot(\alpha))}$$

With $C_\alpha = \sqrt{1 - icot(\alpha)}$, $\alpha = \frac{p\pi}{2}$ and ‘ p ’ is order of the FRFT. If order $p = 0$ or 4, then $\alpha = \frac{p\pi}{2} = 0$ or 2π , and

$$F^0[s(x_1)] = S(x) = \int_{-\infty}^{\infty} \sqrt{1 - icot(0)} e^{-i\pi(2\frac{x_1x}{\sin(0)} - (x^2 + x_1^2) \cot(0))} s(x_1) d(x_1)$$

Where $\sqrt{1 - icot(0)} e^{-i\pi(2\frac{x_1x}{\sin(0)} - (x^2+x_1^2) \cot(0))} = \frac{\infty}{\infty}$, so limit is applied and the resultant equals to $\delta(x_1 - x)$. This implies $F^0=F^4=I$, where I is an identity operator. If order $p = 1$, then $\alpha = \frac{p\pi}{2} = \frac{\pi}{2}$, and

$$F^1[s(x_1)] = S(x) = \int_{-\infty}^{\infty} \sqrt{1 - icot\left(\frac{\pi}{2}\right)} e^{-i\pi\left(2\frac{x_1x}{\sin\left(\frac{\pi}{2}\right)} - (x^2+x_1^2) \cot\left(\frac{\pi}{2}\right)\right)} s(x_1) d(x_1)$$

$$S(x) = \int_{-\infty}^{\infty} e^{-i\pi(2\pi x_1 x)} s(x_1) d(x_1) = \text{Fourier Transform}$$

Where $\sqrt{1 - icot\left(\frac{\pi}{2}\right)} = 1$ and $e^{-i\pi\left(2\frac{x_1x}{\sin\left(\frac{\pi}{2}\right)} - (x^2+x_1^2) \cot\left(\frac{\pi}{2}\right)\right)} = e^{-i\pi(2\pi x_1 x)}$

Similarly, $F^2=P$ and $F^3=FP=PF$, where P is a parity operator. According to this definition, the zero-order transform of a function is the same as the function itself $s(x_1)$, the first order transform is the Fourier transform of $s(x_1)$, and the $\pm 2^{\text{nd}}$ order transform equals $s(-x_1)$. It satisfies important properties such as linearity, Unitary (F^a)⁻¹ = (F^a)^{*}, Index Additivity $F^a F^b = F^{a+b}$, Commutativity $F^a F^b = F^b F^a$, and Associativity ($F^a F^b$) $F^c = F^a (F^b F^c)$.

A rectangular pulse centered at X having a duration of Y is defined as

$$x(u) = \text{rect}\left(\frac{u - X}{Y}\right) = U\left(t - X + \frac{Y}{2}\right) - U\left(t - X - \frac{Y}{2}\right) \quad \dots (2.12)$$

Where U(t) is unit step function. FT of rectangular pulse is Sinc function.

Figure 2.5 depicts real and imaginary parts of fractional transformation of rectangular pulse centered at 0sec with duration of 4secs for various orders. In Figure 2.5, the y-axis represents the amplitude and x-axis depicts normalized neutral axis. The discussion for normalized neutral axis is included in subsequent chapters. Notice how the rectangular pulse is gradually converted into Sinc function with increasing transform order. Periodic nature of FRFT operator implies that the range of α and the order of the transform can be restricted to $\alpha \in [0, 2\pi)$ and order $\in [0, 4)$ respectively. Since the FRFT is a rotation operation on the time frequency distribution, the range of α can be further reduced to $[0, \pi]$ for even symmetric signals. This result holds for most real signals since we can assume that $s(x_1) = s(-x_1)$ for $x_1 < 0$.

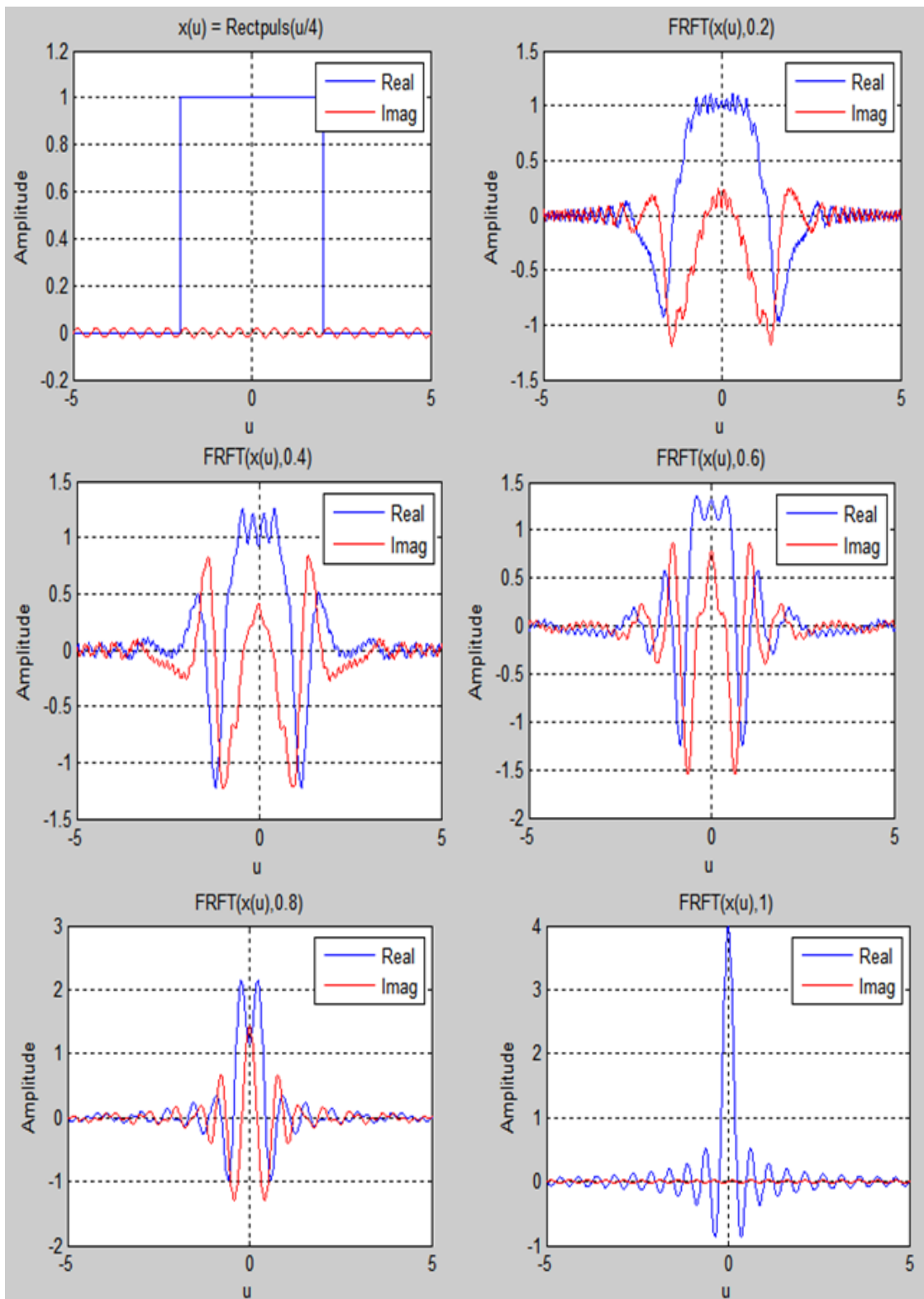


Figure 2.5—FRFT of Rectangular Pulse for Orders 0, 0.2, 0.4, 0.6, 0.8 and 1

2.4 Fractional Fourier Transform Numerical Computation

Conventional Fourier Transform has the advantage of clear physical interpretation, Fast Algorithm (Fast Fourier Transform, FFT) and complexity equal to $(N/2) \log_2(N)$. Fractional Fourier Transform on the other hand has many computation methods and each method satisfies some of the properties mentioned earlier. First method involves direct computation in which input and output can be directly sampled. Although it is easier to implement but it lacks closed form properties, additive, unitary, reversible property and has limited applications. Another method is using chirp convolution method which is implemented by two chirp multiplications and a chirp convolution.

Another method is similar to DFT computation in which signal is first multiplied by a chirp signal, then scaled. Fourier Transform of the scaled signal is taken and finally again it is multiplied by a chirp signal. Complexity of Chirp Convolution method is $2P$ (required for 2 chirp multiplications) + $P \cdot \log_2 P$ (required for 2 DFTs) $\approx P \cdot \log_2 P$ ($P = 2M+1 =$ the number of sampling points). 1 chirp convolution needs to 2DFTs. Complexity of DFT like method is 2 M -points multiplication operations and 1 DFT i.e., $2P$ (two multiplication operations) + $(P/2) \cdot \log_2 P$ (one DFT) $\approx (P/2) \cdot \log_2 P$. In chirp like method there is no constraint on sampling interval while DFT like method puts some constraint for the sampling intervals to be $\Delta_t \Delta_u = 2\pi/P$ where time interval is Δ_t and Δ_u is bandwidth.

Discrete Fractional Fourier Transform can be computed by sampling the continuous FRFT and computing it directly which is the simplest way. Ozaktas and Arikan [9] proposed improved sampling type DFRFT. It has the advantage of being a fast algorithm but kernel function is not orthogonal and additive. Santhanam and MacClellan [10] proposed linear combination type DFRFT based on four bases DFT, IDFT, Identity and Time inverse. It has the advantage of orthogonal transform matrix, additive property and reversible property but loose the 'fractionalization'. Pei et. al. [11] proposed eigenvectors decomposition type DFRFT which is good in removing chirp noise. Richman and Parks proposed group theory type DFRFT in which DFT and periodic chirps were multiplied and it satisfied the rotation property of Wigner distribution, additive and reversible property. Its biggest limitation is that it works only for some specified angles and number of points N should be prime. Arikan,

Kutay and Ozaktas proposed another algorithm known as impulse train type DFRFT. Constraints include signal is normalized but many properties of the FRFT exists. Pei and Ding further improved sampling type of DFRFT, their algorithm is known as closed form DFRFT.

2.5 Wigner Distribution

For a given signal $x(t)$, the corresponding Wigner distribution is defined as

$$W(t, \omega) = \frac{1}{2\pi} \int_{-\infty}^{+\infty} x^* \left(t - \frac{1}{2}\tau \right) x \left(t + \frac{1}{2}\tau \right) e^{-j\tau\omega} d\tau \quad \dots (2.13)$$

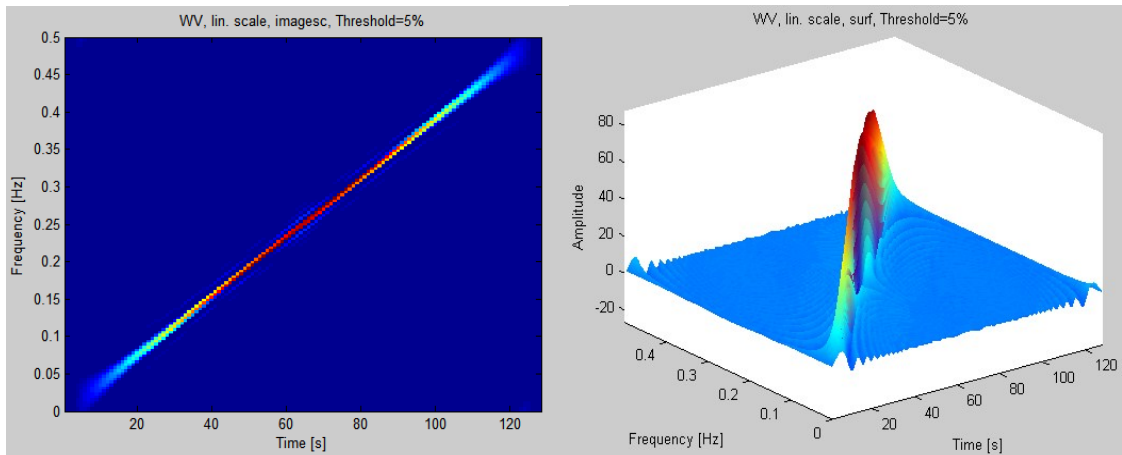
Or

$$W(t, \omega) = \frac{1}{2\pi} \int_{-\infty}^{+\infty} X^* \left(\omega + \frac{1}{2}\theta \right) X \left(\omega - \frac{1}{2}\theta \right) e^{-j\tau\theta} d\theta \quad \dots (2.14)$$

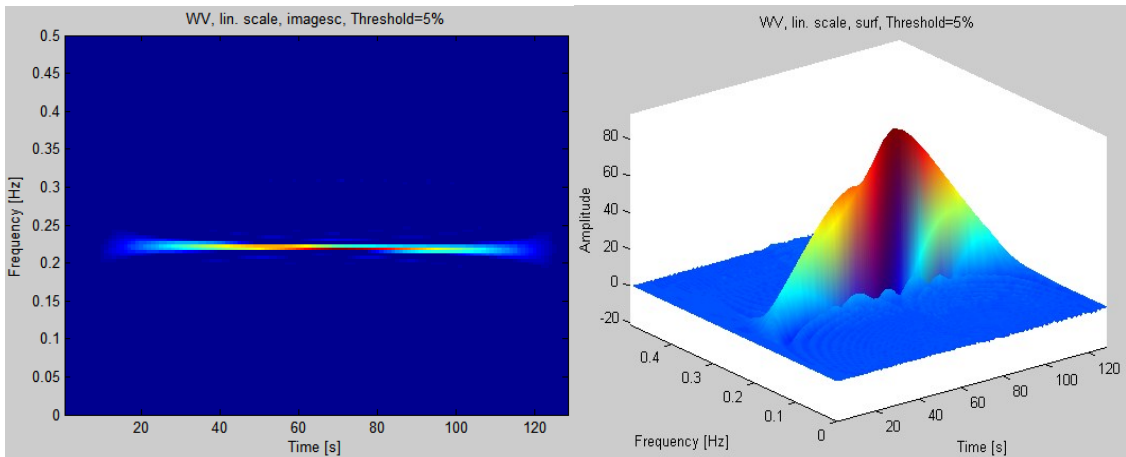
where $X(\omega)$ is the spectrum of the given signal $x(t)$. 'Wigner-Ville Distribution' is defined as the Wigner Distribution where $x(t)$ is the analytic signal of $s(t)$. The analytic signal $x(t)$ of a signal $s(t)$ is defined as $x(t)=s(t)+iH[s(t)]$, where $H[s(t)]$ is the Hilbert Transform of the signal $s(t)$ [12]. Wigner Distribution (WD) of single component chirp signal is given by:

$$W(t, \omega) = \delta(\omega - \omega_0 - \mu_0 t)$$

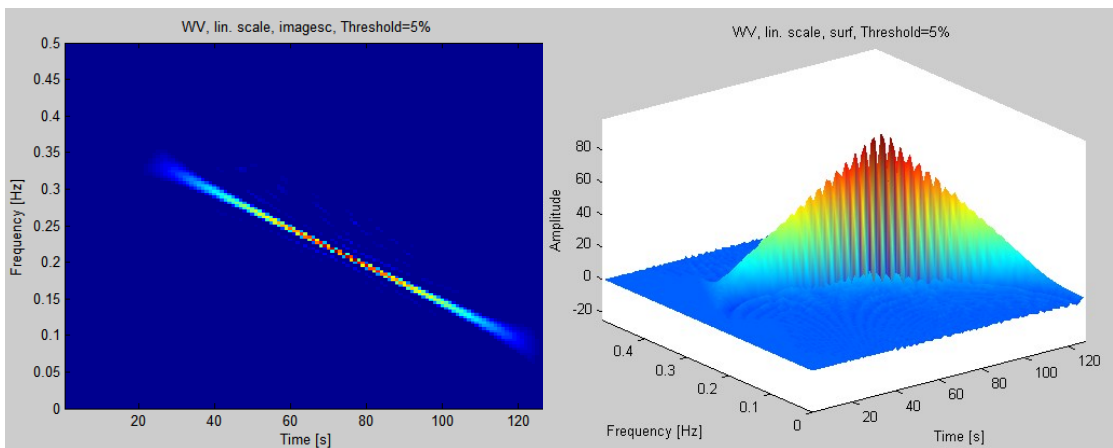
Wigner-Ville Distribution of a chirp signal as an image and its 2-D representation in time-frequency plane is shown in Figure 2.6a while the Wigner-Ville representation of Fractional transformation of the same signal to orders 0.3 and 0.5 is shown in Figure 2.6b and Figure 2.6c respectively.



(a) Representation for Fractional Order = 0



(b) Representation for Fractional Order = 0.3



(c) Representation for Fractional Order = 0.5

Figure 2.6–Rotation of Time-Freq.
Representation of Chirp Signal

Notice how the signal’s frequency is linearly increasing and also being rotated corresponding to various fractional orders. If we apply FRFT on the example signal shown for fractional order 0.3, the chirp signal will be transformed into a peaked function and can be easily detected even in the presence of unwanted signals and interferences. A detailed analysis of this concept is provided in subsequent chapters.

2.6 EEG based BCI System for Person Authentication

Brain Computer Interface (BCI) is a system that enables users to control devices by means of electrical activity, caused by neuronal interactions in the brain, known as

Electroencephalogram (EEG). The amplitude of EEG signal typically lies in the range of $1\mu\text{V}$ to $100\mu\text{V}$ for a normal adult when recorded at the scalp and is improved to 2mV to 10mV if recorded at sub-Dural level. The frequency band is typically taken in the range of 0.1 to 100Hz. This frequency band is sub-divided into delta band (0.1-3Hz), theta band (4-7Hz), alpha band (8-12Hz), low beta band (12-15Hz), midrange beta band (16-20Hz), high beta band (21-30Hz) and gamma band (30-100Hz). A BCI system in essence records EEG signals using electrodes; user envisions performing a task and resultant EEG signals are interpreted by BCI system to perform control action.

For instance if a user imagines moving his right hand, a BCI system will similarly move a wheel chair in right direction. There are generally two types of BCI systems; Synchronous BCIs and Asynchronous BCIs. Synchronous BCIs detect user activity spontaneously and consequently performs the control action [13]. User is not required to follow cues by the system which provides for a more user friendly interface but is considerably more difficult to build. Main issues fuelling this difficulty are sensitivity of the sensors and efficiency of algorithm to detect between significant and trivial brain activity. Asynchronous BCIs on the other hand requires regular system cues for the user to perform activity. System only responds to activity during cue time. Online BCI systems work in real time; users have to maintain a continuous connection to a signal acquisition machine whereas offline analysis is performed on pre-recorded datasets to test efficiency of algorithms. Current trends in online BCI approach indicates the use of unipolar electrode to capture EEG signals for electric wheel chair control through Bluetooth interface [14], use of eye blinks (major artifact in EEG) as a control signal to control Virtual Keyboard using the LabVIEW platform [15] and online spelling interface based on P300 wave in EEG signal [16].

2.6.1 Biometric System

A Biometric system is a system used to uniquely recognize humans based on their physical and biological characteristics like DNA, Ear, Face, Finger print etc. A Biometric system is generally either used for Person Identification or Authentication. Person Identification involves matching a single person's EEG features from a set of many templates corresponding to different users in the database, whereas an

Authentication / Verification system verifies claimed identity of an individual against a single user template.

2.6.2 Brain Computer Interface Composition

Brain Computer Interface (BCI) based Biometric system comprises of five main parts. The block diagram of a typical Brain Computer Interface system is shown in Figure 2.7.

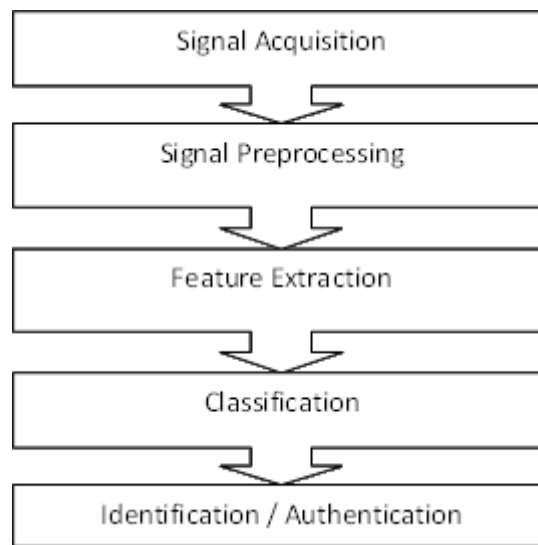


Figure 2.7–Block Diagram of typical BCI Based Biometric System

First part is multi-channel signal acquisition system, which records and amplifies Electroencephalogram (EEG, Brain Signals) or any other signals from the brain. It also performs common mode noise elimination and artifact processing etc.

Then a pre-processing block is used with the aim to bring the signals into a suitable or compatible form for feature extraction block. The feature extraction block in BCI based Biometric System extracts such features that are unique for an individual; the pattern is repeatable, universal, not time dependent and is acquirable. Existing EEG systems used for user identification includes, Poulos et al. [17] who tried to differentiate four subjects individually from a pool of different individuals using autoregressive (AR) models to model EEG signal and then using the parameters of the AR model for the identification. Palaniappan et al. [18] investigated features based on the spectral power of the signal. Se'bastien et al. [19] proposed an approach based on

Gaussian Mixture Models and Maximum A Posteriori model adaptation from features based on Fourier Transform for person authentication.

Feature vectors formed by Feature extraction block, are used by classification block, in classifying the signals. When designing a BCI, the feature extraction and the classification algorithm is vitally important as the behaviour of BCI is decided by the classification algorithm directly [20]. However advances in technology have made it possible to record and process EEG data from 128 different electrodes and brain locations. This has raised an important issue of selection of appropriate number of relevant channels for a particular brain activity and how the information from these channels will be processed.

The automated approach to selection of relevant channel for motor imagery tasks based on support vector machine (SVM) and for person identification based on independent component analysis (ICA) were proposed in [21], [22] respectively. As for information processing from multi-channel EEG, one approach is to concatenate the features from multiple electrodes into one feature vector after feature reduction and input the resultant vector to a classifier [2], [3]. Another approach is to use parallel structure of electrodes where each electrode is connected to an independent classifier, and final classification decision is made on the results of individual classifiers using simple majority rule [23]. After the classification block there is the Identifier / Verifier block which translates the classification of the previous block into identifying or authenticating the user.

2.7 Summary

To summarize, in this chapter an introduction to chirp signal was provided in relation to the drawbacks of Fourier Transform. FRFT was introduced and transform of rectangular window for various fractional orders was carried out to demonstrate how rectangular pulse signal is transformed into a Sinc function. Brain Computer Interface and its various blocks especially the existing work carried out in the feature extraction were also discussed. Subsequent chapters will build up on the information presented in this chapter.

FRACTIONAL FOURIER TRANSFORM APPLICATIONS

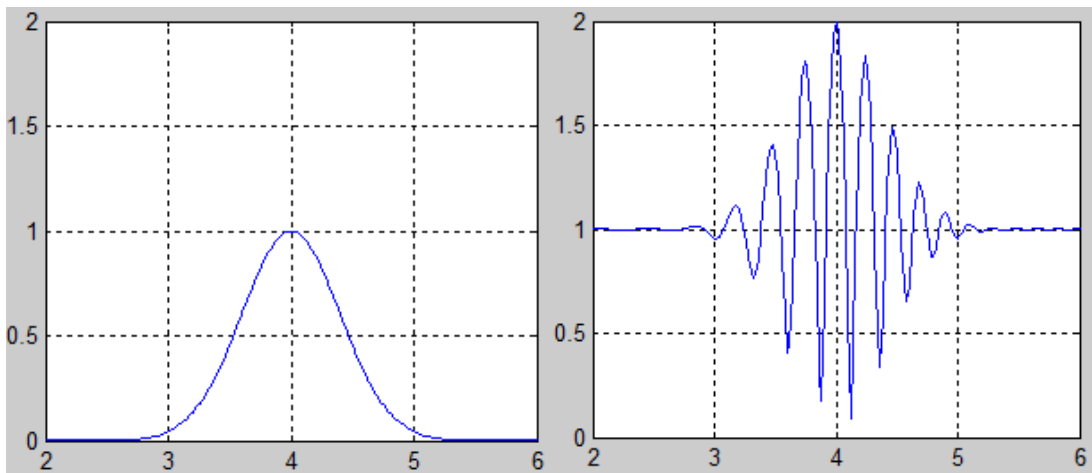
3.1 Introduction

In this chapter, summarized work and analysis of various research papers that includes Filtering in Fractional Fourier Domain by Ozaktas et. al. [24], Practical Normalization Techniques by Xinghao et. al. [25], Maximum Amplitude Method for Compact Fractional Fourier Domain (MACF) Algorithm by Zheng et. al. [26], and FRFT for Biomedical Signal Detection by Zhang et. al. [27], is presented and discussed in detail. Results shown in this chapter are all Mathworks Matlab® simulations carried out of the research papers mentioned above.

3.2 Filtering in Fractional Fourier Domain

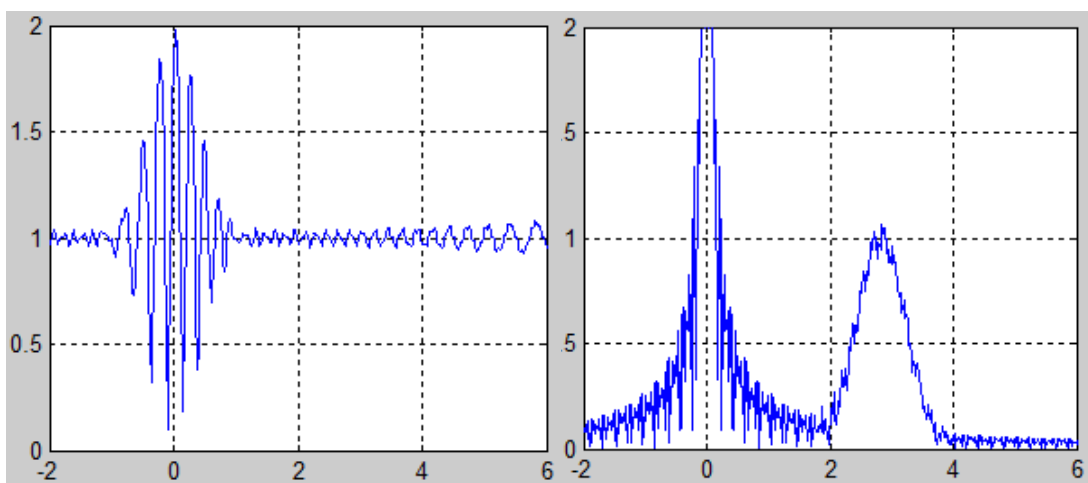
Signals passing through electronic equipment suffer from distortion due to noise. In some cases conventional filtering techniques applied either fail to completely remove the noise from the signal or causes degradation to the original signal since both the noise signal and original signal components overlap in time and frequency domain. In such cases FRFT can be used to recover the original signal by finding an optimum order which results in separation of noise and signal components.

Consider the Gaussian pulse signal $x(t) = e^{-\pi(t-4)^2}$ distorted additively by $n(t) = e^{-i\pi t^2} \text{rect}(t/16)$ where $\text{rect}(t/16)$ is rectangular function with time width 16 centered at origin. The original signal, magnitude of the sum of original signal and distortion, original and noise signal overlap representation in frequency domain, signal separation in Fractional domain for order 0.5, application of masking filter and original vs. recovered signal are shown in part (a) to (f) of Figure 3.1 respectively.



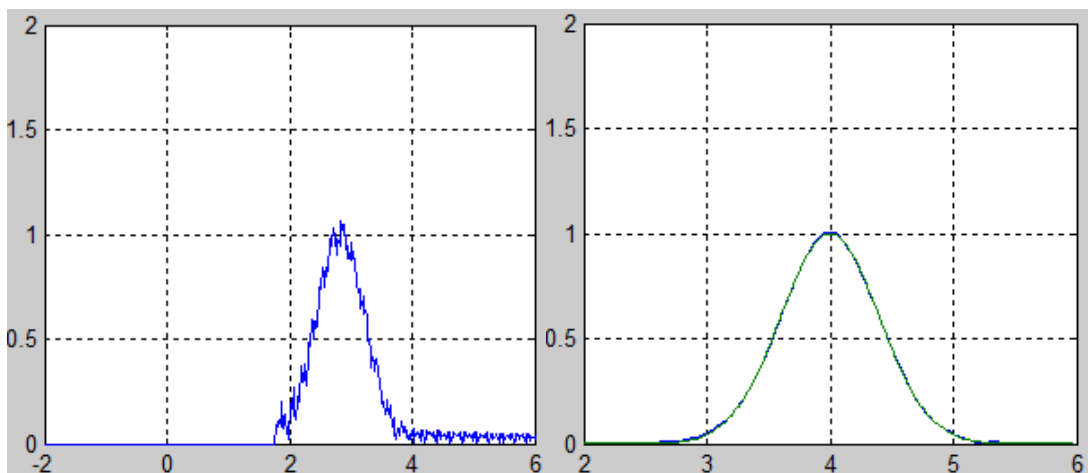
(a) Original Signal

(b) Distorted Signal



(c) FT of Distorted Signal

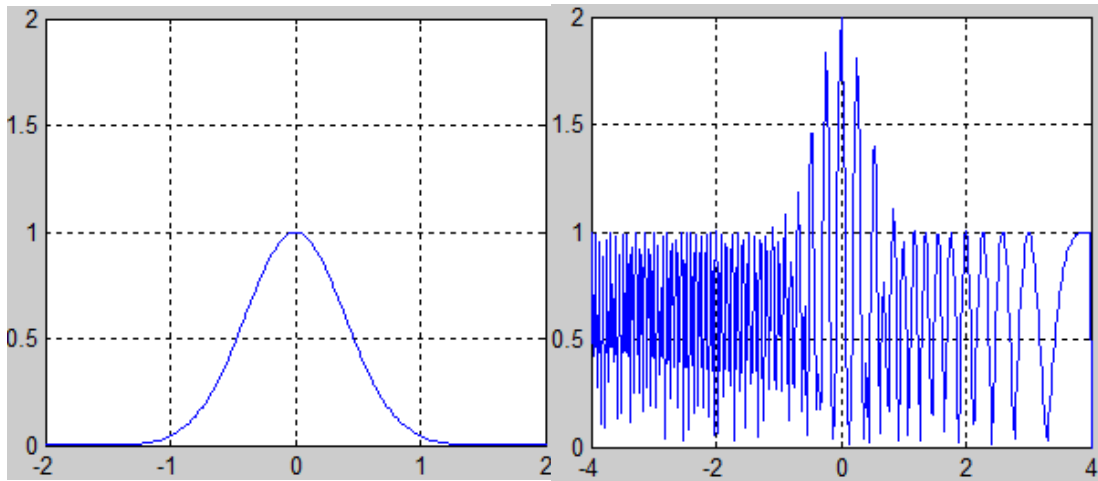
(d) FRFT of Distorted Signal, ($p = 0.5$)



(e) Masking Filter Applied

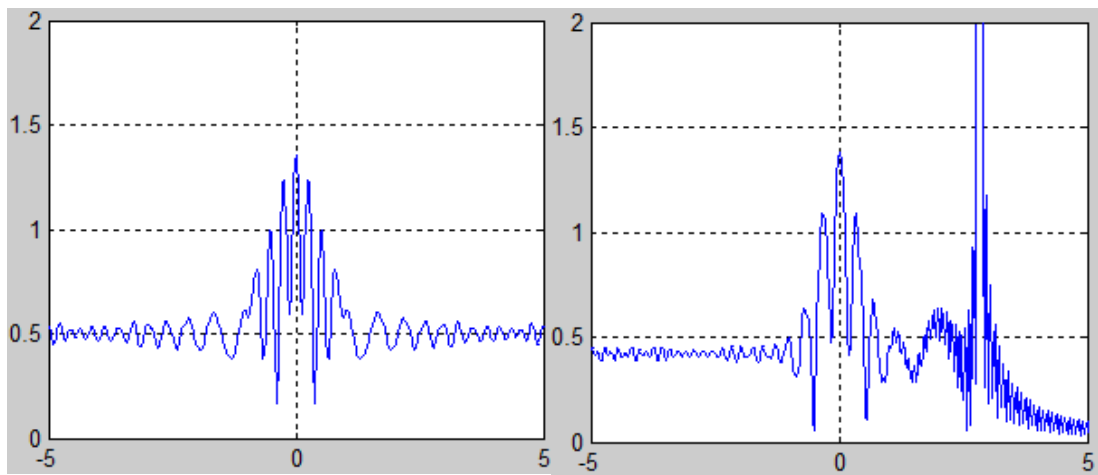
(f) Original Signal vs. Recovered Signal

Figure 3.1–Filtering in Fractional Domain
Example 1



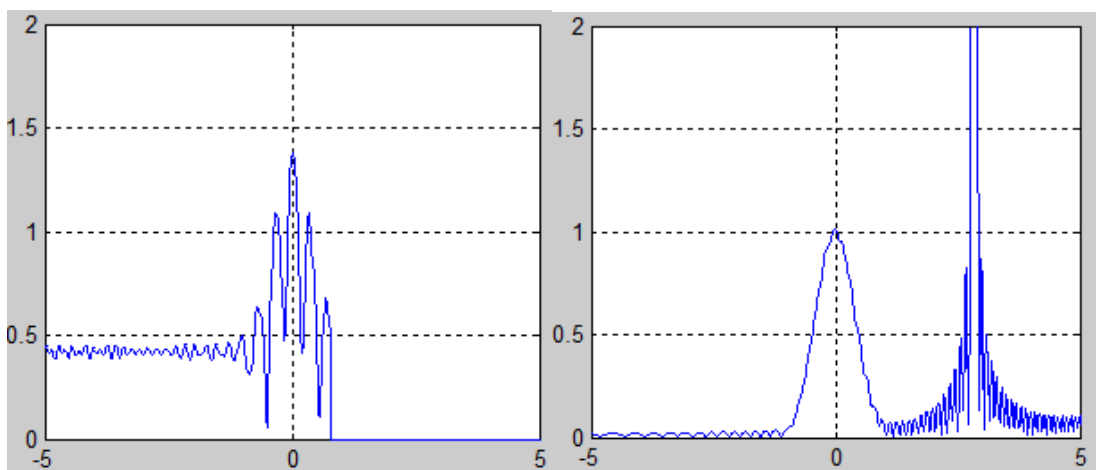
(a) Original Signal

(b) Distorted Signal



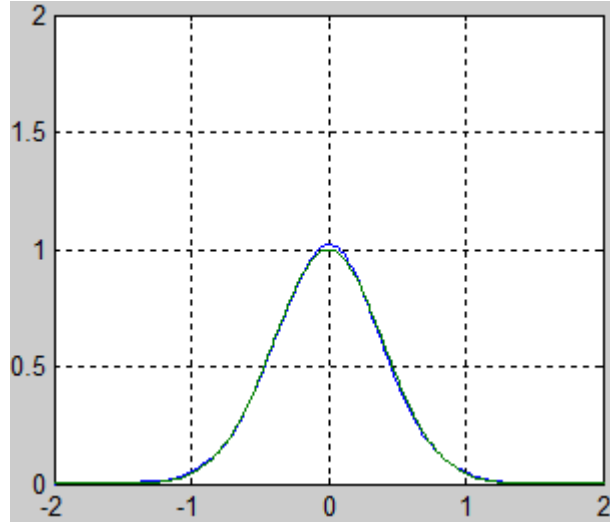
(c) FT of Distorted Signal

(d) FRFT of Distorted Signal,
(Order $p = 0.5$)



(e) Masking Filter Applied

(f) Another FRFT, (Order $p = -1$)



(g) Original Signal vs. Recovered Signal

Figure 3.2–Filtering in Fractional Domain
Example 2

Figure 3.2 illustrates another example for filtering in fractional domain. Consider another signal $e^{-\pi t^2}$ is again distorted additively but this time by a real signal $\cos[2\pi(\frac{t^2}{2} - 4t)]rect(\frac{t}{8})$. Since original signal in this example suffers from greater distortion compared to the previous example as shown in Figure 3.2b, multiple FRFT have been applied to recover the original signal back. FRFT of order 0.5 is applied on the distorted signal shown in Figure 3.2d, one component of cosine chirp distortion is transformed into a peaked function without any significant overlap with the original signal and is masked out as shown in Figure 3.2e. Another FRFT of order -1 (inverse FT) is applied to transform the signal to $p = -0.5^{\text{th}}$ domain, which separates out the remaining distortion in the signal and is masked out and another FRFT of order 0.5 is applied to recover the original signal back without any discernible distortion.

The results obtained in Figure 3.1 and Figure 3.2 can only be achieved for sampling frequency of 50Hz and signal time duration of $[-25 \ 25]$. These values were not mentioned in the research work implemented and were only discovered on the basis of hit and trial. This raised an obvious question about the relationship between frequency and time duration of the signal and its impact on the Fractional order.

3.3 Dimensional Normalization

As mentioned earlier, FRFT rotates the Wigner distribution of a signal from time to frequency axis and is a linear distribution hence the horizontal axis in fractional domain represented in Figure 3.1 and Figure 3.2 is dimensionless. Let us consider that intervals $[-\frac{\Delta t}{2}, \frac{\Delta t}{2}]$ and $[-\frac{\Delta f}{2}, \frac{\Delta f}{2}]$ confines time domain and frequency domain representations of our signal respectively that is Δt and Δf are significantly large so that the signal energy outside of this interval approaches zero. The length of both these intervals is made equal to a dimensionless quantity $\Delta x = \sqrt{\Delta t \Delta f}$ by selecting a scaling parameter $S = \sqrt{\Delta t / \Delta f}$ with the dimension of time. The scaling results in new dimensionless coordinates (x, v) with

$$x = t/S, v = f.S \quad \dots (3.1)$$

The signal is confined to a new interval $[-\frac{\Delta t}{2S}, \frac{\Delta t}{2S}] = [-\frac{\Delta f.S}{2}, \frac{\Delta f.S}{2}] = [-\frac{\Delta x}{2}, \frac{\Delta x}{2}]$. Applying the sampling theorem to normalized signal provides us $N = \Delta t \Delta f = \Delta x^2$ samples with sampling interval equal to $1/\Delta x$, where N is the time bandwidth product.

The whole process defined above is known as Dimensional Normalization and is a prerequisite to the application of FRFT to a signal. However in most practical situations only observation time and sampling frequency for the discrete observation data of the original signal is known which limits the use of normalization in its current form. To mitigate this problem there exist two techniques in literature and both of them are described below.

3.3.1 Discrete Scaling Method (DSM):

The essential condition in DSM is to select time width Δt , bandwidth Δf , scaling factor S and normalized width Δx in such a manner that the total number of samples N (Time-Bandwidth Product) before and after the normalization remains the same. This is achieved through equating time width Δt equal to observation time T (where midpoint of the observation data is taken as time origin) and bandwidth Δf equal to sampling frequency f_s , resulting in time domain and frequency domain representations

of the signal to be confined to $\left[-\frac{T}{2}, \frac{T}{2}\right]$ and $\left[-\frac{f_s}{2}, \frac{f_s}{2}\right]$ interval respectively. Once time width and bandwidth are known scaling factor S and normalized width Δx can be deduced as follows:

$$S = \sqrt{\frac{\Delta t}{\Delta f}} = \sqrt{\frac{T}{f_s}} \quad \dots (3.2)$$

$$\Delta x = \sqrt{\Delta t \Delta f} = \sqrt{T \cdot f_s} \quad \dots (3.3)$$

It is obvious that by applying the scaling factor found above to observation data using Eq. (3.1) changes the sampling interval to $1/\Delta x$ and confines the data to $\left[-\frac{\Delta x}{2}, \frac{\Delta x}{2}\right]$ interval.

3.3.2 Data Zero Padding/Interception Method (DZPIM):

The signal deformity and distortion caused as a result of normalization in the previous method can be avoided by setting the scaling factor S equal to 1 and both the normalized width Δx and the bandwidth Δf are made equal to sampling frequency f_s which is only possible if and only if time width $\Delta t = f_s$. But in most practical situations $\Delta t = T \neq f_s$ so in order to satisfy the condition $\Delta t = f_s$ we can have two possible scenarios i.e. either $f_s > T$ or $f_s < T$.

Case I: ($f_s > T$)

In this case the original signal is confined to $\left[-\frac{T}{2}, \frac{T}{2}\right]$ and in order to make it equal to $\left[-\frac{\Delta x}{2}, \frac{\Delta x}{2}\right] = \left[-\frac{f_s}{2}, \frac{f_s}{2}\right]$ interval, time width of the data is increased artificially by padding it with zeros in the interval $\left[-\frac{f_s}{2}, -\frac{T}{2}\right]$ and $\left[\frac{T}{2}, \frac{f_s}{2}\right]$ with sampling interval equal to the original sampling interval. This method of normalization is known as data zero padding method (DZPM).

Case II: ($f_s < T$)

Here time range of the original signal which lies in the interval $\left[-\frac{T}{2}, \frac{T}{2}\right]$ is decreased to the interval $\left[-\frac{\Delta x}{2}, \frac{\Delta x}{2}\right] = \left[-\frac{f_s}{2}, \frac{f_s}{2}\right]$ by discarding the data outside of this interval. This method of normalization is known as data interception method (DIM).

In both the examples demonstrated in Figure 3.1 & Figure 3.2 the sampling frequency $f_s = 50 < T$. Using DZPM the interval of the signals is artificially increased by padding zeros in the intervals $[-25 - 8]$ and $[8 25]$ in case of example 1 increasing the original sample size from 800 to 2500 samples and $[-25 - 4]$ and $[4 25]$ in case of example 2 increasing the original sample size from 400 to 2500 samples making the intervals equal to $-25:0.02:25$.

As evident from these examples, this method of normalization does not introduce distortion in the signal but has the disadvantage of huge interception of data values or padding of zeros that are required if the difference between sampling frequency f_s and time width T is large making it impossible to use for real time applications due to excessive computational load of FRFT.

3.4 Chirp Signal Parameter Estimation and Optimum Order

A chirp signal can be estimated if the Fundamental Frequency f_o and Chirp Rate μ_o of the signal are known. Both of these parameters can be determined using FRFT since a chirp signal with specific chirp rate has maximum amplitude for the corresponding fractional domain and the resultant fractional order is termed as optimum order.

In order to determine the optimum order FRFT of the signal for the entire range of fractional order $p \in [0 2]$ is evaluated and a 2-dimensional parametric plane (p, u) consisting of distribution of signal energy along fractional domain u and fractional order p is obtained. Then second-order central Fractional FT moment is used to estimate \hat{u}_o and \hat{p}_o defined by Eq. (3.4) and Eq. (3.5) which is associated with principle axis with fractional angle ' α ' [1].

$$P_{1\alpha} = \int_{-\infty}^{\infty} |X_{\alpha}(u)|^2 (u - m_{1\alpha})^2 du \quad \dots (3.4)$$

Where $m_{1\alpha}$ is the first order moment and is defined as:

$$m_{1\alpha} = \int_{-\infty}^{\infty} |X_{\alpha}(u)|^2 u du \quad \dots (3.5)$$

$$P_{2\alpha} = \int_{-\infty}^{\infty} |X_{\alpha}(u)|^2 (p - m_{\alpha})^2 du \quad \dots (3.6)$$

Where $m_{2\alpha}$ is the first order moment and is defined as:

$$m_{2\alpha} = \int_{-\infty}^{\infty} |X_{\alpha}(u)|^2 p du \quad \dots (3.7)$$

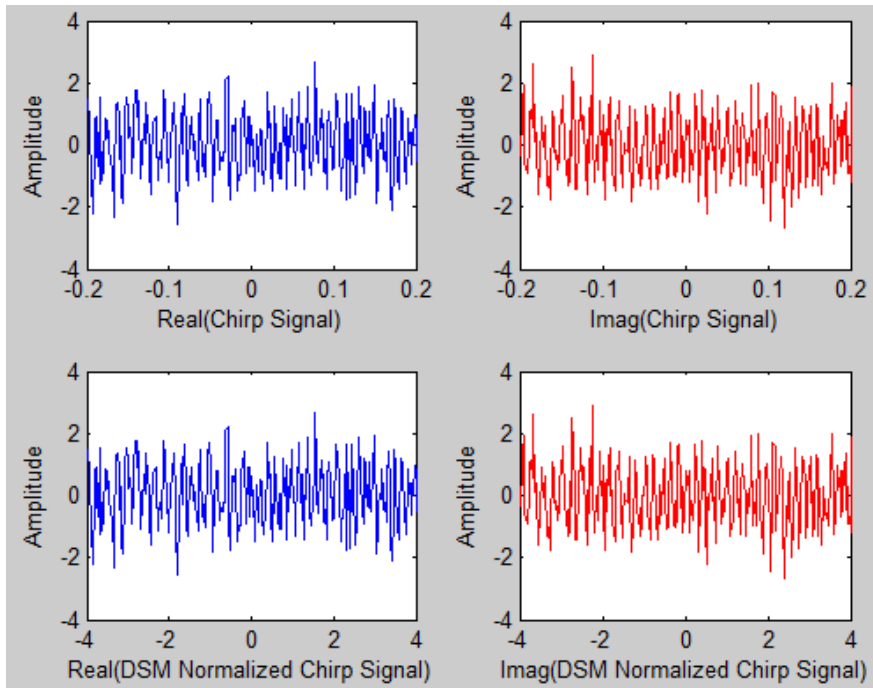
The parameters \hat{u}_o and \hat{p}_o has a relationship with Chirp Rate μ'_o and Fundamental Frequency f'_o of the dimensionally normalized signal and is defined as:

$$\begin{cases} \mu'_o = -\cot\left(\frac{\hat{p}_o\pi}{2}\right) \\ f'_o = \hat{u}_o \csc\left(\frac{\hat{p}_o\pi}{2}\right) \end{cases} \quad \dots (3.8)$$

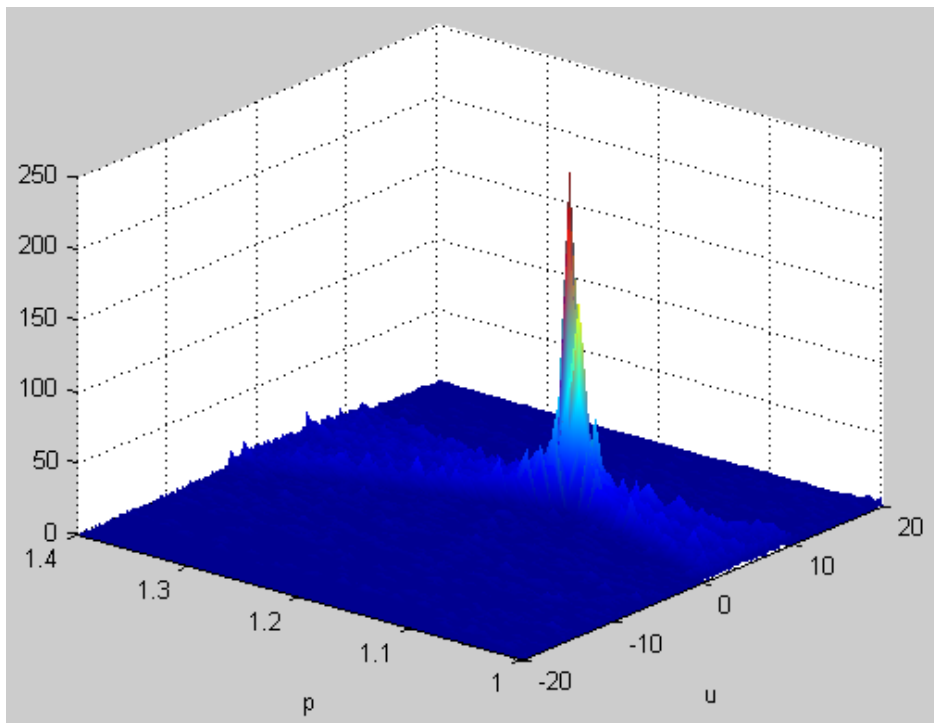
If μ_o and f_o are Chirp Rate and Fundamental Frequency of the signal before normalization respectively, then using Eq. (3.1) and Eq. (3.2) they can be estimated as:

$$\begin{cases} \mu'_o = \frac{v}{x} = \frac{f \cdot S}{t/S} = \mu_o \cdot S^2 = \mu_o T / f_s \\ f'_o = f_o \cdot S = f_o \sqrt{T/f_s} \end{cases} \quad \dots (3.9)$$

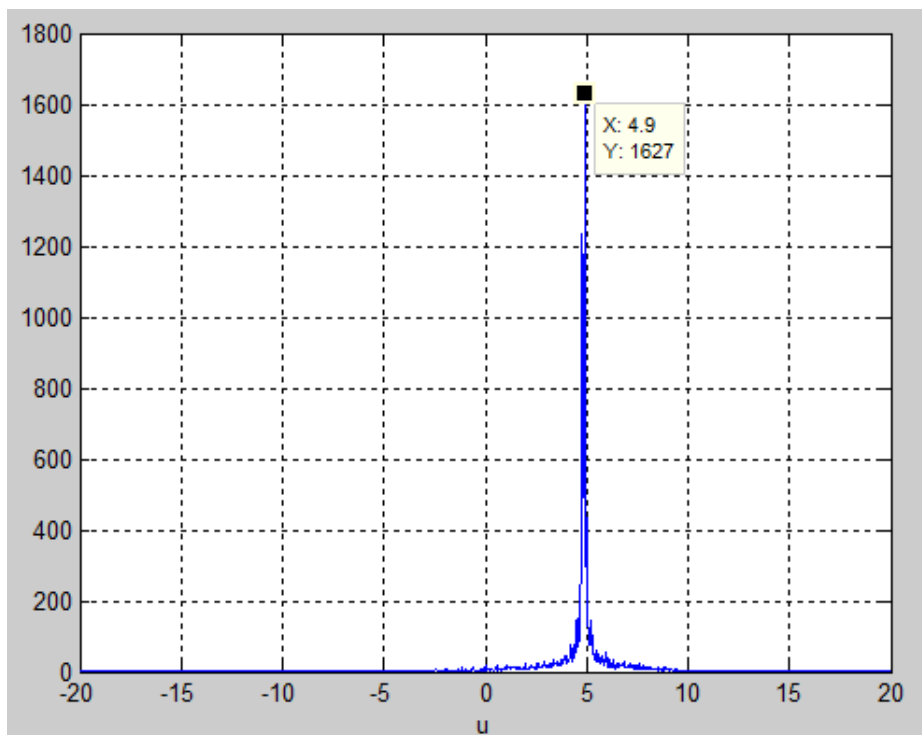
Therefore Eq. (3.9) provides a relationship for Chirp Rate and Fundamental Frequency of the signal before and after the dimensional normalization. An example of DSM normalization with parameter estimation is shown in Figure 3.3.



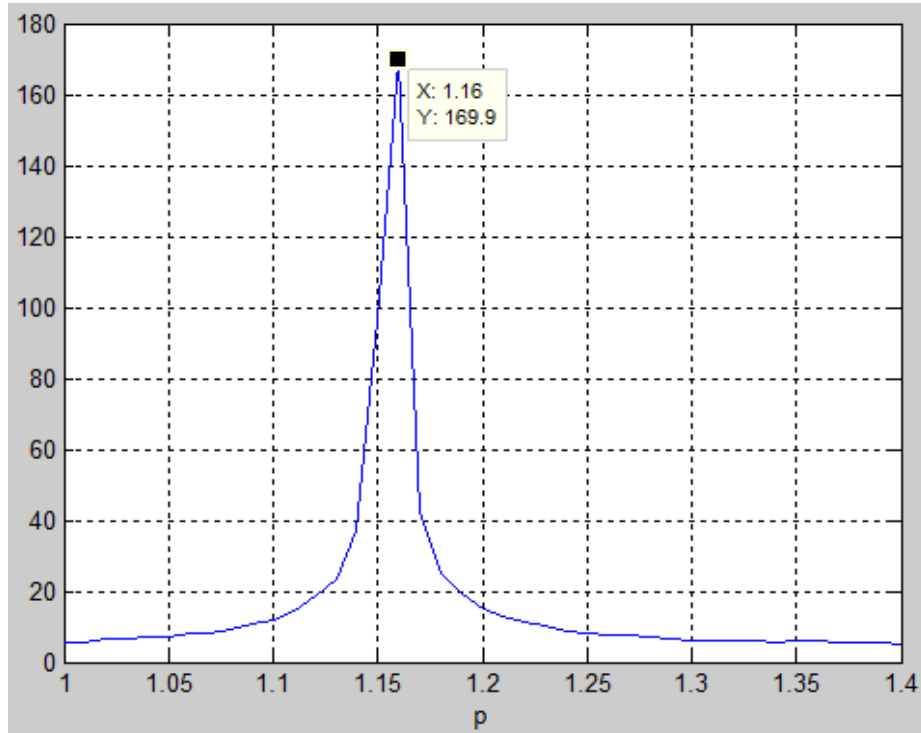
(a) Real and Imaginary Parts of Original and Dimensionally Normalized Chirp Signal distorted by AWGN noise



(b) Two Dimensional Parametric Plane (p, u)
containing $|X_\alpha(u)|^2$



(c) P_{1_α} to estimate \hat{u}_o



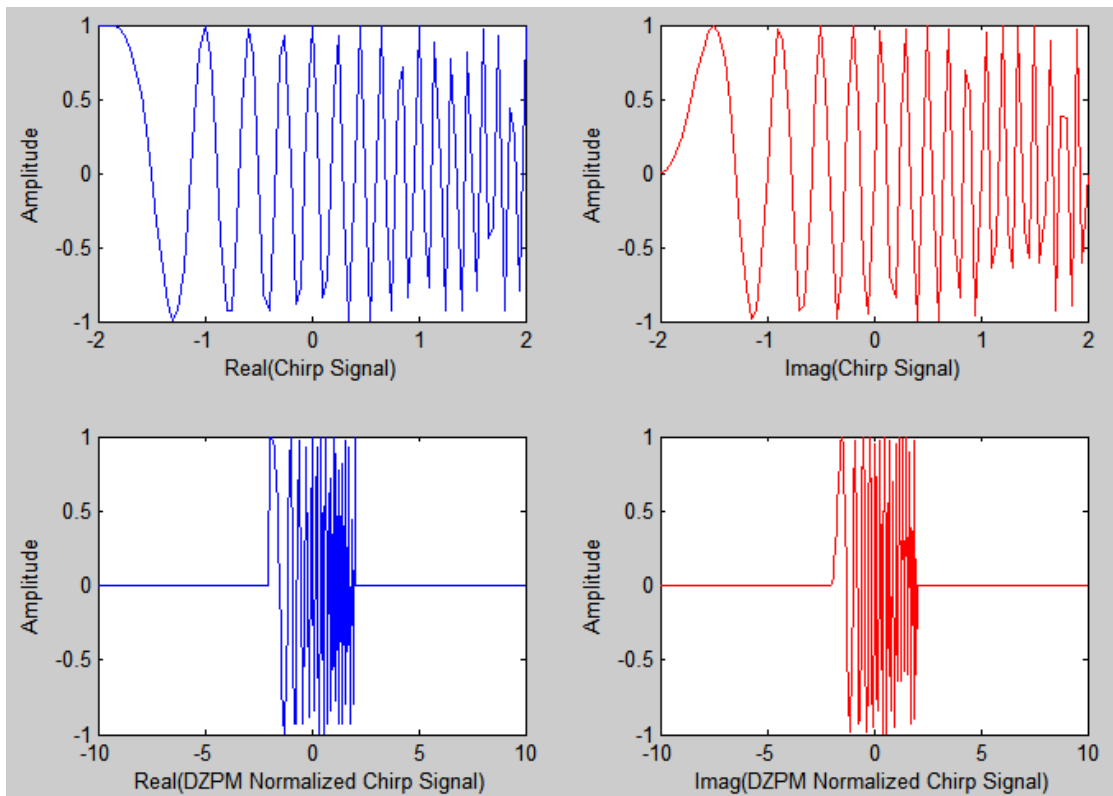
(d) $P_{2\alpha}$ to estimate \hat{p}_o

Figure 3.3–Effect of Dimensional Normalization (DSM) on Chirp Parameters Example 1

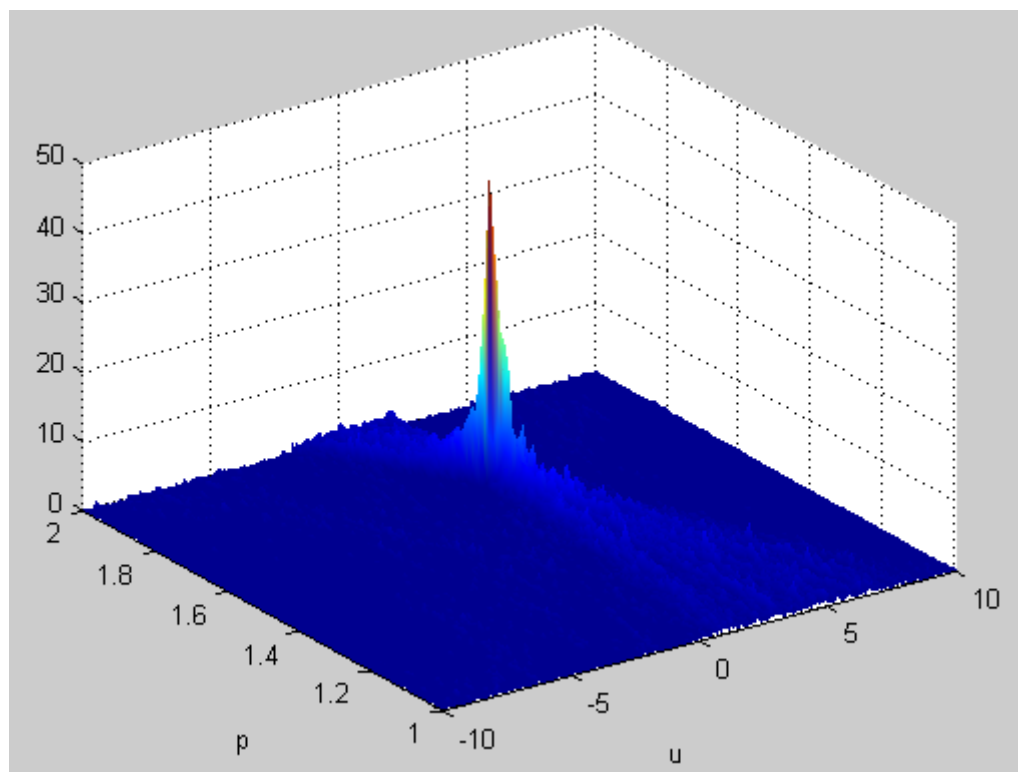
Let's consider a chirp signal with Observation Time $T = 2s$, Sampling Frequency $f_s = 800\text{Hz}$, Fundamental Frequency $f_0 = 100\text{Hz}$ and Chirp Rate $\mu_0 = 100\text{Hz/s}$ and $\text{SNR} = 0\text{dB}$ 'measured'. The signal is dimensionally normalized with DSM since $f_s \gg T$. Using Eq. (3.2) we get Scaling Factor $S = 0.05s$ and from Eq. (3.3) we get $\Delta x = 40$ which provides dimensionless interval equal to $[-20\ 20]$. From Eq. (3.9) we calculate the Chirp Rate $\mu'_0 = 0.25$ and Fundamental Frequency $f'_0 = 5$ of the dimensionally normalized signal.

Figure 3.3a shows a small portion of Original and Dimensionally Normalized Chirp Signal. Two dimensional parametric plane (p, u) representing FRFT for order $p \in [1\ 1.4]$ and $u = [-20\ 20]$ with $\hat{u}_o = 4.9$ and $\hat{p}_o = 1.16$ is shown in Figure 3.3b – 3.3d respectively. Using Eq. (3.8) Normalized Chirp Rate $\mu'_0 = 0.2568$ and Fundamental Frequency $f'_0 = 5.0589$. Therefore, using Eq. (3.9) actual chirp parameters are estimated to be $f_0 = 101.178\text{Hz}$ and $\mu_0 = 102.72\text{Hz/s}$.

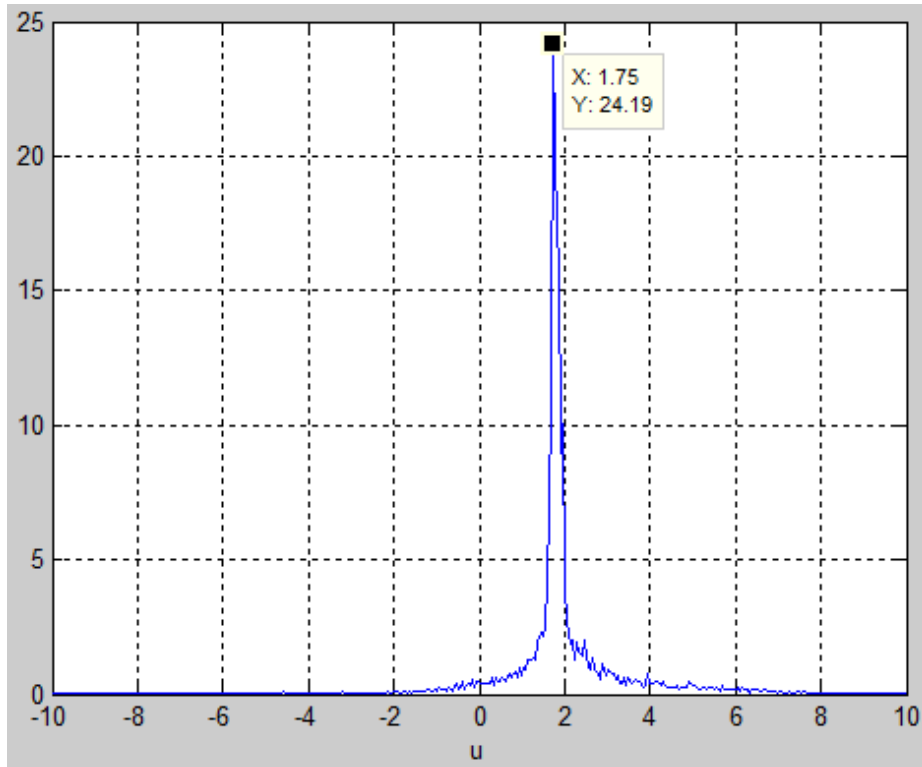
Another example of chirp signal but with DZPM normalization and parameter estimation is shown in Figure 3.4.



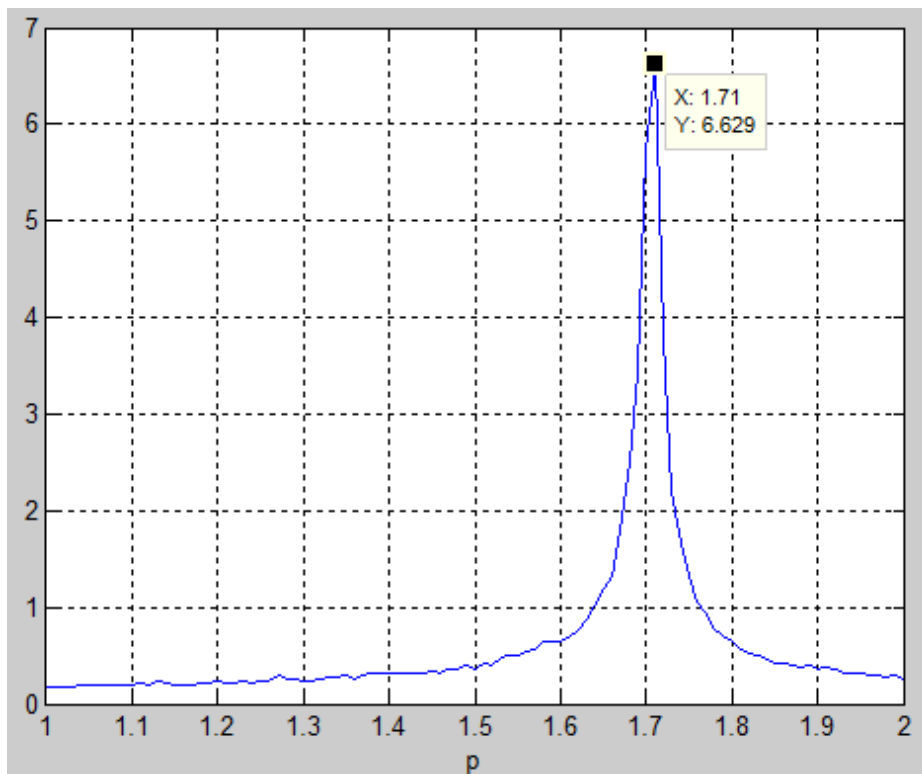
(a) Real and Imaginary Parts of Original and Dimensionally Normalized Chirp Signal



(b) Two Dimensional Parametric Plane (p, u) containing $|X_\alpha(u)|^2$



(c) $P_{1\alpha}$ to estimate \hat{u}_o



(d) $P_{2\alpha}$ to estimate \hat{p}_o

Figure 3.4—Effect of Dimensional Normalization (DZPM) on Chirp Parameters
Example 2

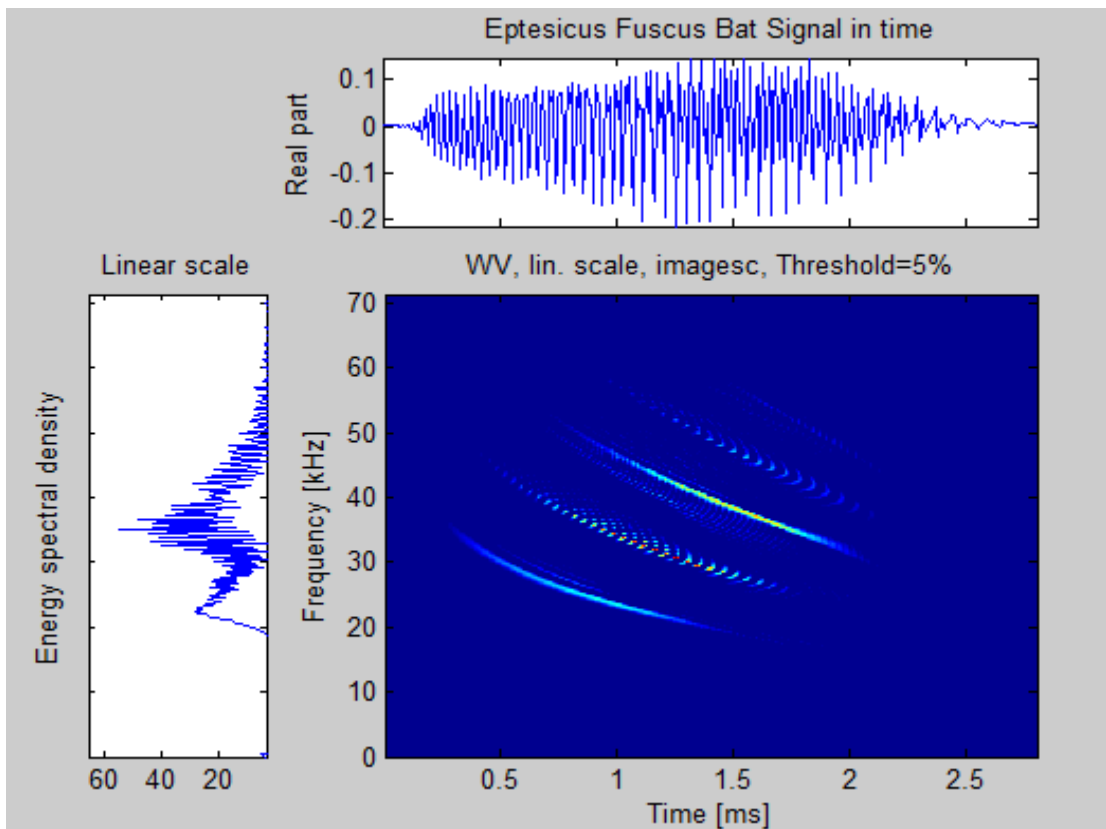
Lets consider a Chirp Signal with Observation Time $T = 4s$, Sampling Frequency $f_s = 20\text{Hz}$, Fundamental Frequency $f_0 = 4\text{Hz}$ and Chirp Rate $\mu_0 = 2\text{Hz/s}$ and $\text{SNR} = 0\text{dB}$. In this example $f_s > T$ but the difference is not too large therefore we will dimensionally normalize the original chirp signal using DZPM. Here Scaling Factor $S = 1s$ and $\Delta x = 20$ which provides dimensionless interval equal to $[-10 \ 10]$. The interval $[-10 \ -2]$ and $[2 \ 10]$ is padded with zeros at the sampling interval $1/\Delta x$. DZPM does not affect the Chirp Rate μ'_0 and Fundamental Frequency f'_0 of the original chirp signal. Figure 3.4a shows Original and Dimensionally Normalized Chirp Signal. Two dimensional parametric plane (p, u) representing FRFT for order $p \in [1 \ 2]$ and $u = [-10 \ 10]$ with $\hat{u}_o = 1.75$ and $\hat{p}_o = 1.71$ is shown in Figure 3.4b – 3.4d respectively. Therefore, using Eq. (3.9) actual chirp parameters are estimated to be $f_0 = 3.9778\text{Hz}$ and $\mu_0 = 2.0413\text{Hz/s}$.

3.5 Maximum Amplitude Method for Compact FRFT Domain (MACF)

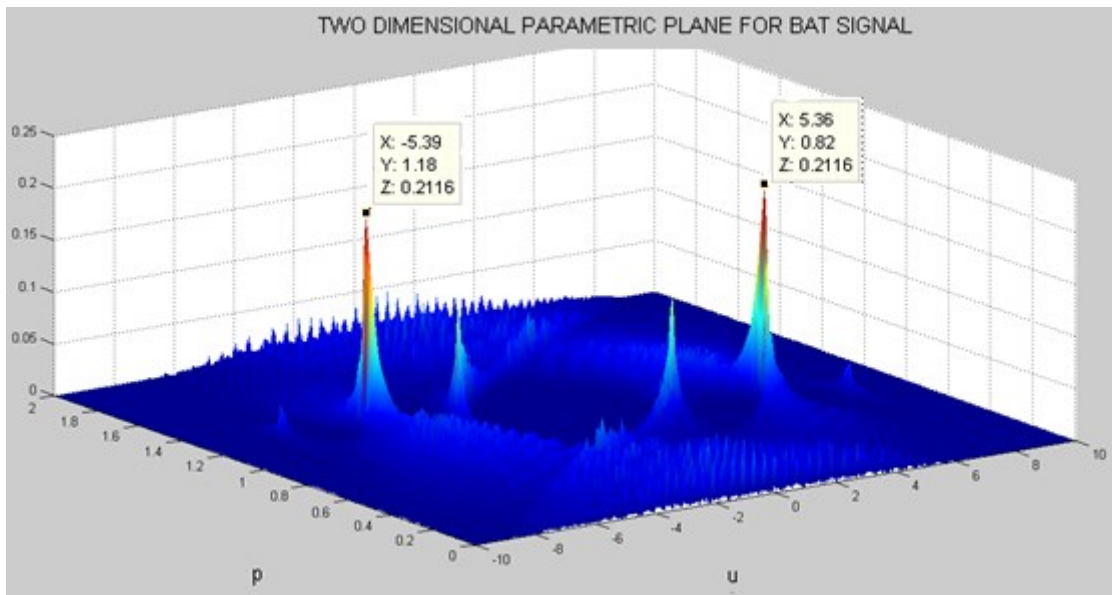
In the examples discussed so far, a two dimensional parametric plane was obtained through exhaustive search i.e. after evaluating the FRFT of the signal for each order in the range $[0 \ 2]$ making this approach time consuming. Since FRFT is a unitary transformation and is continuous with respect to the transform order, Zheng et. al. proposed a coarse to fine algorithm in order to reduce the computational time and used this approach to estimate compact Fractional Fourier domain.

Using the Time-Frequency representation rotation property and its periodic nature, order of the transform is first reduced to $[0 \ 4]$. Using the Index Additivity property of the transform, order is further reduced to $[0 \ 2]$ i.e., $F^a F^b = F^{a+b}$ or as an example $F^{3.5} = F^{2+1.5} = F^2 F^{1.5}$. Authors of the research paper reduced this range even further to $[0 \ 1]$ by assuming the signal to be even symmetric as in case of most real signals it can be presumed that $f(t) = f(-t)$ for $t < 0$. This assumption by the authors does not remain valid if DZPM dimensional normalization is applied on the observation data since it takes midpoint of the available data as the time origin which might not necessarily be even symmetric. DSM is not considered here as it operates only along time dimension thereby not affecting the optimum order.

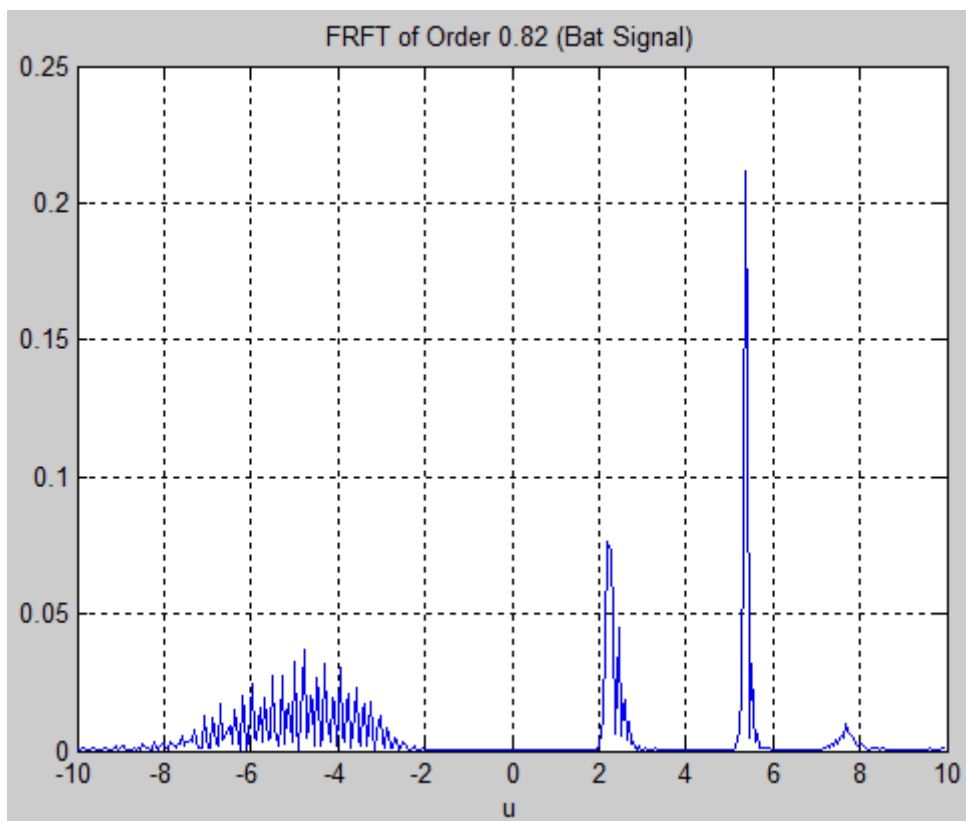
If the signal energy value is zero outside a smallest interval around the origin for a particular order than the corresponding fractional domain is considered to be compact. Since FRFT satisfies the Parseval's theorem which states that signal energy is independent of fractional order which implies that for a compact Fractional Fourier domain $|F^\alpha|^2$ will have maximum value of all the orders. Also Index Additivity property implies that F^α is continuous with respect to α therefore instead of evaluating for entire range of orders in the interval $[0, 2]$, we begin with a large initial step size Δp_i between two consecutive evaluated fractional orders and find the maximum energy concentration. Then Δp_i is reduced to a smaller range in a small region around the order. These steps are repeated till the difference of energy concentration of two consecutive orders is either equal to zero or less than preset small value ϵ . This approach has the advantage of lower computational load compared to the exhaustive search in the previous technique. MACF algorithm was applied to 400 recorded samples of digitized echolocation pulse emitted by the Large Brown Bat at sampling period of $7\mu\text{secs}$ and the results are shown in Figure 3.5.



(a) Time Domain, Frequency Domain and Wigner Time-Frequency Representation



(b) Two Dimensional Parametric Plane for Digitized Echolocation Pulse of Large Bat



(c) Result of Fractional Fourier Transform of Order 0.82 for Bat Signal

Figure 3.5—Optimum Order for Signal emitted by Large Brown Bat

Real part of the bat signal in Time Domain, Energy Spectral density in Frequency Domain and its Wigner-Ville Time-Frequency Representation as an image is shown in Figure 3.5a. Figure 3.5b represents the 2-D parametric plane to estimate optimum order through exhaustive search. Optimum order p is found to be 0.82 as can be seen from Figure 3.5b along y-axis. X-axis represents normalized neutral axis u and z-axis represents the amplitude of the two dimensional parametric plane representation. The fractional order of the signal was found to be 0.82 using MACF and is similar to the results obtained using exhaustive search approach. Figure 3.5c shows the Fractional Fourier Transform representation of order 0.82 for the bat signal under consideration. The MACF algorithm approach proposed was also tested for all the examples presented in previous sections and the results were similar to the ones found through exhaustive approach.

3.6 FRFT for Biomedical Signal Detection

Biomedical signals are extremely weak signals and are corrupted by external noise sources (50Hz mains hum) and other interferences like artifacts (eye blinks). The obtained signal $x[n]$ can be modeled as:

$$x[n] = s[n] + w[n] + I[n] \quad \dots (3.10)$$

Where $s[n]$ is the original signal, $w[n]$ is the noise usually assumed to be AWGN, and $I[n]$ is interferences from surrounding sources independent with $s[n]$ and $w[n]$. Application of FRFT to Eq. (3.10) results in the following expression:

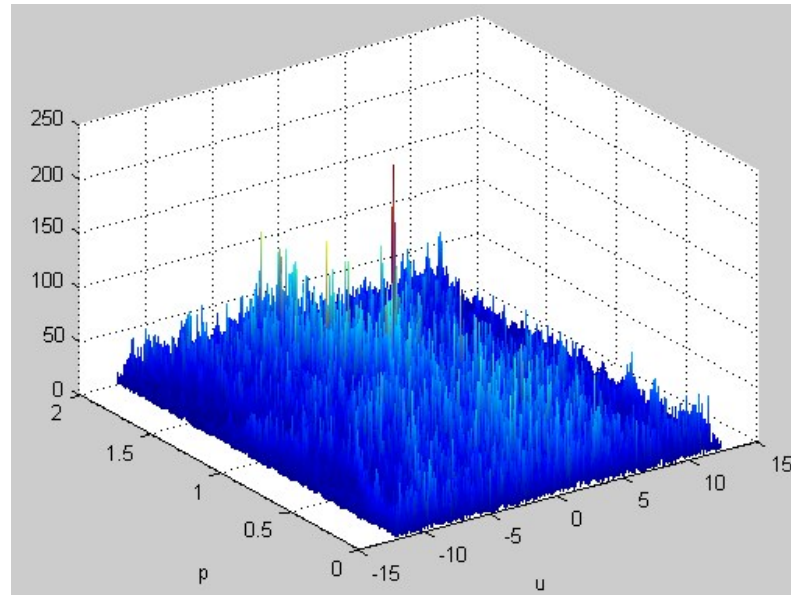
$$X_\alpha(u_k) = S_\alpha(u_k) + W_\alpha(u_k) + I_\alpha(u_k) \quad \dots (3.11)$$

Where $X_\alpha(u_k)$, $S_\alpha(u_k)$, $W_\alpha(u_k)$ and $I_\alpha(u_k)$ represents FRFT of $x[n]$, $s[n]$, $w[n]$ and $I[n]$ respectively.

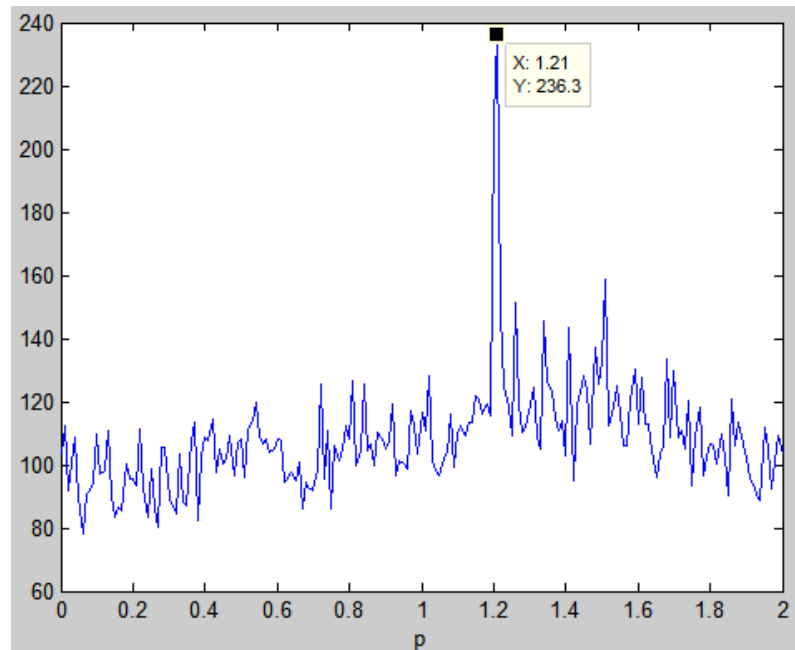
As stated earlier, “a signal can be regarded as the linear combination of a set of orthonormal chirps functions with high concentration in the principle axis” [27], therefore two examples with both single component and multi-component chirp signal are demonstrated in the simulations.

Let $x(t)$ be composed as in Eq. (2.1) with $w(t) =$ AWGN with SNR= -9.5dB with

Chirp Rate $\mu_0 = 2\text{Hz/s}$, Fundamental Frequency $f_0 = 1\text{Hz}$ and Sampling Frequency = 60Hz within the interval $[0\ 10]$. The signal is dimensionally normalized and then a two dimensional parametric plane is obtained as shown in Figure 3.6.



(a) Two dimensional Parametric Plane



(b) $P_{2\alpha}$ to estimate \hat{p}_o

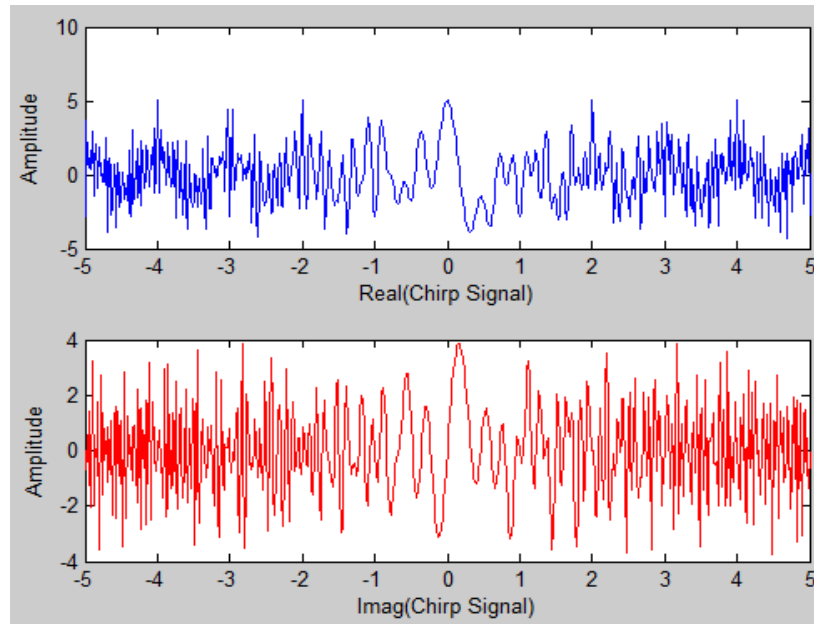
Figure 3.6–Biomedical Signal Detection in presence of AWGN noise

As can be seen from the Figure 3.6 chirp signal is transformed into a peak function making it easier to detect while AWGN noise energy remains as it is.

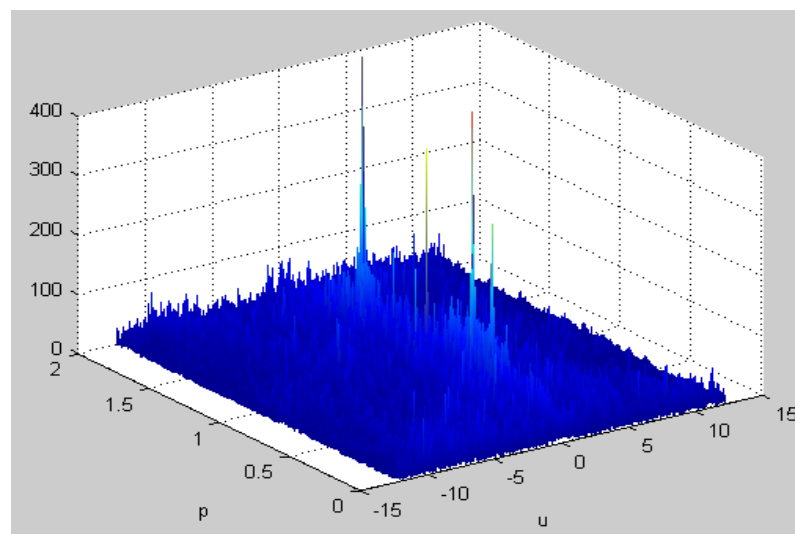
In the second example $x(t)$ is composed of Multi-Component chirp signals with no change in observation time and sampling frequency.

$$x(t) = s_1(t) + s_2(t) + I_1(t) + I_2(t) + w(t) \quad \dots (3.12)$$

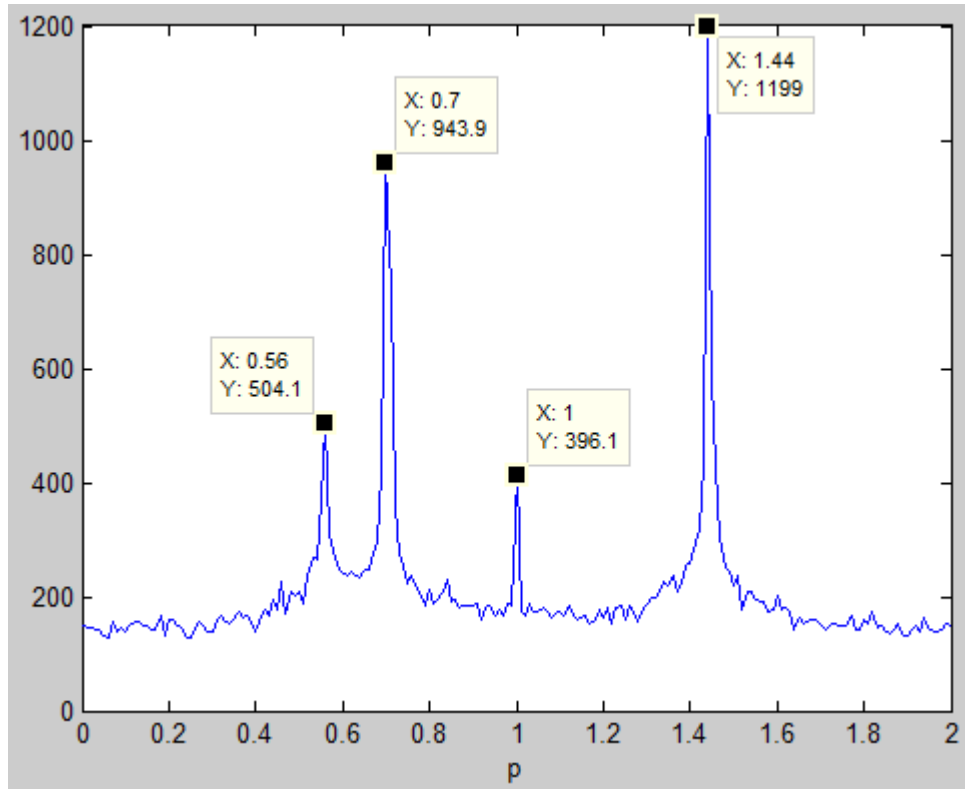
Where $s_1(t) = 1.5 \exp(i2\pi t + i5\pi t^2)$, $s_2(t) = 1.2 \exp(i4\pi t - i3\pi t^2)$, $I_1(t) = 1.2 \exp(i4\pi t + i\pi t^2)$ and $I_2(t) = \cos(2\pi t)$. Using similar approach, as used in the earlier example, results are obtained as shown in Figure 3.7.



(a) Real and Imaginary Parts of Multi-Component Chirp Signal



(b) Two Dimensional Parametric Plane (p, u) containing $|X_\alpha(u)|^2$



(c) $P_{2\alpha}$ to estimate \hat{p}_o

Figure 3.7–Biomedical Signal Detection of Multi-Component Chirp Signal in presence of AWGN noise

In Figure 3.7(b), u is the normalized neutral axis and p is the fractional order. The four peaks depicted in Figure 3.7(b) and Figure 3.7(c) corresponds to each of the chirp signals while AWGN noise energy still remains as it is. With prior knowledge of chirp parameters, interfering signals can be easily separated from original signal components.

3.7 Summary

To summarize this chapter provided a detailed overview of the applications of FRFT to filtering in Fractional domain, Chirp signal parameter estimation and utilization of FRFT and its effectiveness for biomedical signal detection even in the presence of unwanted signals and distortion due to noise.

EXPERIMENTAL SETUP AND ALGORITHM DESIGN FOR PERSON AUTHENTICATION

4.1 Introduction

As mentioned earlier, a typical BCI system comprises of multichannel EEG signal acquisition device, pre-processing, feature extractor, classifier and control interface. In this chapter experimental details of each of these blocks are provided.

4.2 Data Acquisition

Data Acquisition was carried out through EEG signal acquisition device designed indigenously shown in Figure 4.1.



Figure 4.1–EEG Signal Acquisition Device

Another pre-recorded dataset available from Colorado University website [25] was also used for offline analysis to test the efficiency of the algorithm.

4.2.1 EEG Signal Acquisition Device

The signal acquisition device is the actual link between the brain and the computer. The device captures EEG signals either through electrodes placed at the scalp in standard International 10-20 positions, with the help of a conducting gel (non-invasive

approach) or through electrodes surgically implanted in the brain (invasive approach). Signals recorded through invasive approach offers less noise contamination, lower attenuation and higher resolution resulting in higher accuracy BCI systems however higher costs and possible risk of operation makes them unfeasible for widespread use. In non-invasive approach the activity signals to be detected are greatly attenuated by the skull and have typical amplitude of 2-100 microvolts; however with improvements in technology non-invasive techniques are becoming increasingly efficient.

Data was recorded using four gold plated passive electrodes placed at standard International 10-20 system locations C3, C4, P3 and P4 using ECG conducting gel. Another electrode was placed at right ear lobe and was used as reference. Signals from the electrodes were amplified by Analog Devices Instrumentation Amplifier (In-Amp) AD620 with a gain of 11. Gain of the In-Amp was calculated through relation $G = 1 + 50k/R_G$ where R_G was $5k\Omega$, 1% tolerance and $\frac{1}{2}$ Watt power rating external resistor. For future designs Analog Devices In-Amp AD621 with a pre-set gain of 10 will be used since it does not require any external components. Since most EEG activity occurs within the following frequency bands; delta (0.5 - 4 Hz), theta (4-8 Hz), alpha (8-13 Hz), beta (13-30 Hz) and gamma (30-40 Hz), signals from In-Amp are band-limited to 0.5-40Hz [29].

In-Amp AD621 has a reference pin for enabling AC and DC coupling. If Ref pin is grounded, output of In-Amp AD621 is DC coupled (allows all frequencies to pass). However if the output of In-Amp is passed through a low pass filter and returned to Ref pin, signal is AC coupled (DC and low frequencies are cutoff). A simple operational amplifier (op-amp) integrator circuit based on Analog Devices precision operational amplifier OP177 connected between In-Amp output pin and Ref pin with $1\mu\text{F}$ feedback capacitor and $330k\Omega$ input resistance at inverting terminal effectively provides a cutoff frequency of 0.48Hz approximately. For future designs Texas Instruments OPA277 which is an industry upgrade of OPA177 will be used. OPA277 is also available in Quad Op-Amp IC package (OPA4277). AC coupled output of the In-Amp was passed through inverting amplifier with a gain of 60 and a second order Multiple Feedback active low pass filter with a gain of 10 and passband frequency $\approx 40\text{Hz}$. Low-Pass filter and its frequency response is shown in Figure 4.2.

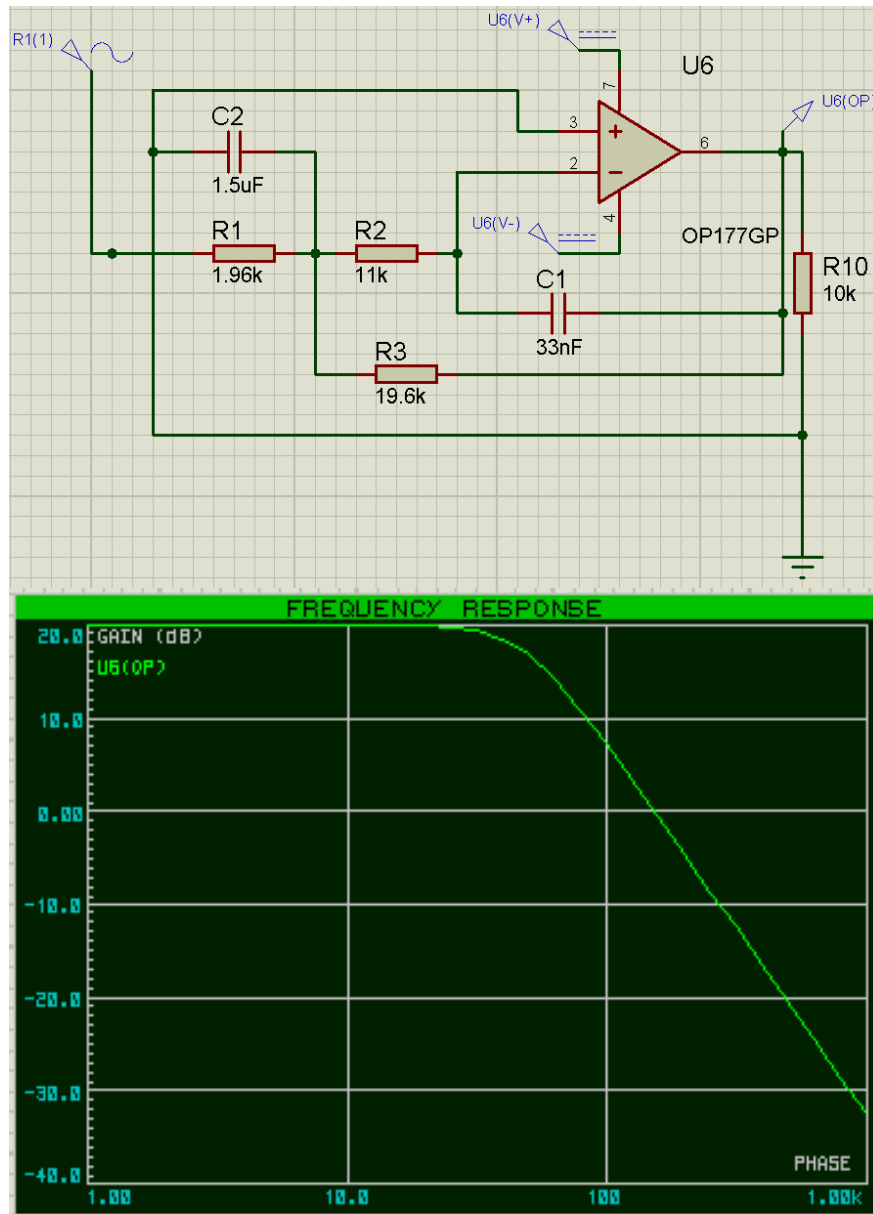


Figure 4.2–Second Order Multiple Feedback Low Pass Filter and its Frequency Response

Overall system gain becomes 6600. Amplified and band limited signals of the four channels were then amplitude modulated to approx. 0.974kHz, 3.210kHz, 5.39kHz, and 6.42kHz center frequencies and summed to form a composite signal. Analog devices AD633 analog multiplier was used for Amplitude modulation and Intersil Americas Inc.'s ICL8038 IC was used for carrier generation. The composite signal was attenuated below 0.6V and using Line-In mode of PC/Laptop sound card signal was acquired. Amplitude Spectrum up to 25kHz of composite signal of four channels acquired is shown in Figure 4.3.

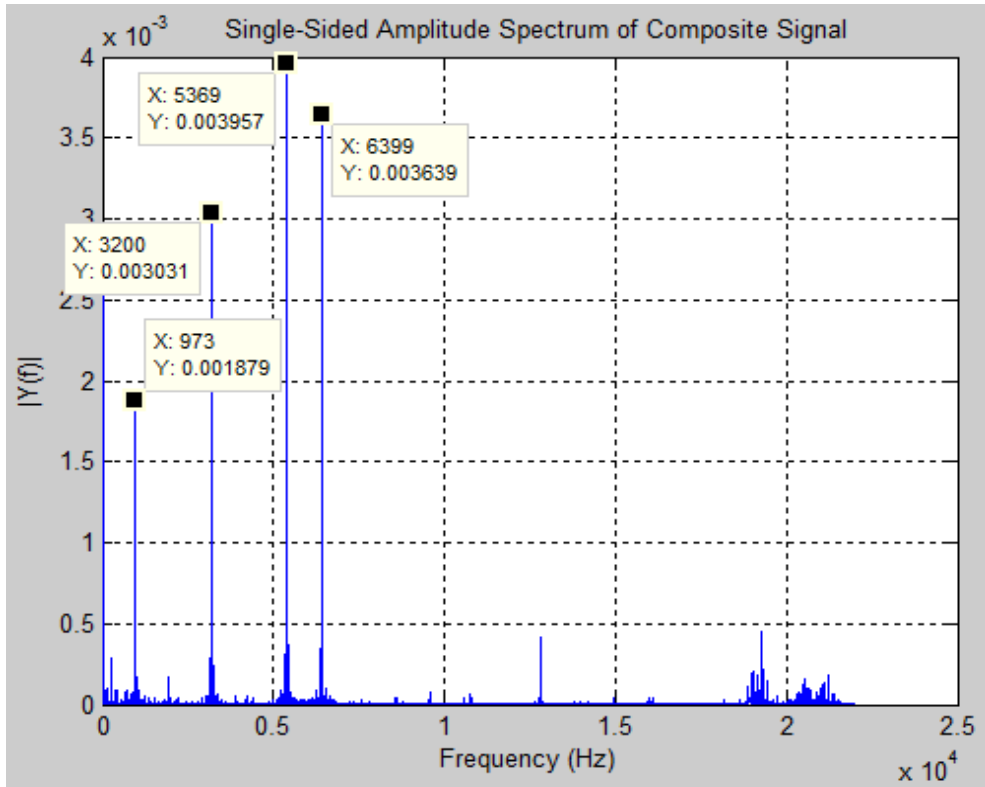


Figure 4.3–Amplitude Spectrum of Composite Signal

4.2.2 Self-Recorded Dataset – I and II

Five color coded electrodes were placed at standard International 10-20 brain locations. Two datasets were recorded. Task performed included mental imagery of right and left movement of both hands and feet. Table 4.1 provides information about color coding, location and modulation frequency for each electrode connected.

Table 4.1–INDIVIDUAL ELECTRODE COLOR CODES & LOCATION

Electrode#	Electrode Color	Brain Locations	Modulation Frequency
E1	Yellow	P3	6.42kHz
E2	Purple	P4	5.39kHz
E3	Black	Reference Right Ear Lobe	-
E4	Brown	C4	3.21kHz
E5	Blue	C3	0.974kHz

Table 4.2–SYSTEM CUES & MOTOR IMAGERY TASKS

Task Performed	Motor Imagery Movement
Right	Right Arm
Left	Left Arm
Up	Left Leg
Down	Right Leg

Table 4.3–SUBJECTS AND TOTAL TRIALS FOR ALL MOTOR IMAGERY TASKS DATASET - I

Subj #	Day I			Day II			Total Trials
	Session I	Session II	Session III	Session I	Session II	Session III	
1	40	40	40	-	-	-	120
2	40	40	40	40	40	40	240
3	40	40	40	40	40	40	240
4	-	-	-	40	40	40	120
Total	120	120	120	120	120	120	720

Table 4.4–SUBJECTS AND TOTAL TRIALS FOR MOTOR IMAGERY TASKS DATASET - II

Subj #	Motor Imagery Task				Total Trials
	Up-Cue	Down-Cue	Left-Cue	Right-Cue	
1	20	20	20	20	80
2	20	20	20	20	80
3	20	20	20	20	80
4	20	20	20	20	80
5	20	20	20	20	80
6	20	20	20	20	80
7	20	20	20	20	80
8	20	20	20	20	80
9	20	20	20	20	80
10	20	20	20	20	80
11	20	20	20	20	80
Total	220	220	220	220	880

The tasks performed and their corresponding mental imagery movements are provided in Table 4.2. Each subject was asked to imagine movement of limbs corresponding to a picture of cursor displayed for duration of 1sec and 2sec for Dataset-I and II respectively. There was a break of 1sec during the consecutive tasks performed. Details of trials performed by each subject of Dataset-I are listed in Table 4.3.

Dataset–I comprised of trials from four subjects performed on two different days in a total of six sessions, three on each day for each subject. There was a break of five minutes between the three consecutive sessions performed for each subject and the electrodes were not removed. In each session five trials for each task were performed.

Details of trials performed by each subject of Dataset–II are listed in Table 4.4. Dataset–II comprised of 11 subjects. Each subject was asked to perform tasks similar to the ones performed in Dataset–I. Twenty Trials were performed in a single session for each task for a total of 880 trials for all the Motor Imagery tasks. Recordings were made on two consecutive days. All the subjects were medically fit male students of the college with ages between 18 and 24 years. Trials of additional two subjects were recorded but were not included in the dataset as they were corrupted due to power failure during the recording session.

4.2.3 Pre-Recorded Colorado University Dataset

EEG signals were recorded by [29] using seven Non-Invasive active electrodes placed at standard International 10-20 system locations C3, C4, P3, P4, O1, O2 and EOG at a sampling frequency of 250Hz from seven individuals, six males and one female. Mastoids A1 and A2 were electrically linked and used as reference. The electrode placed at EOG was used to record the movement of Eye ball. Mental Imagery tasks performed were Baseline Task, Multiplication Task, Letter-composition Task, 3-D Rotation Task and Counting Task. Recorded EEG signals are shown in Figure 4.4.

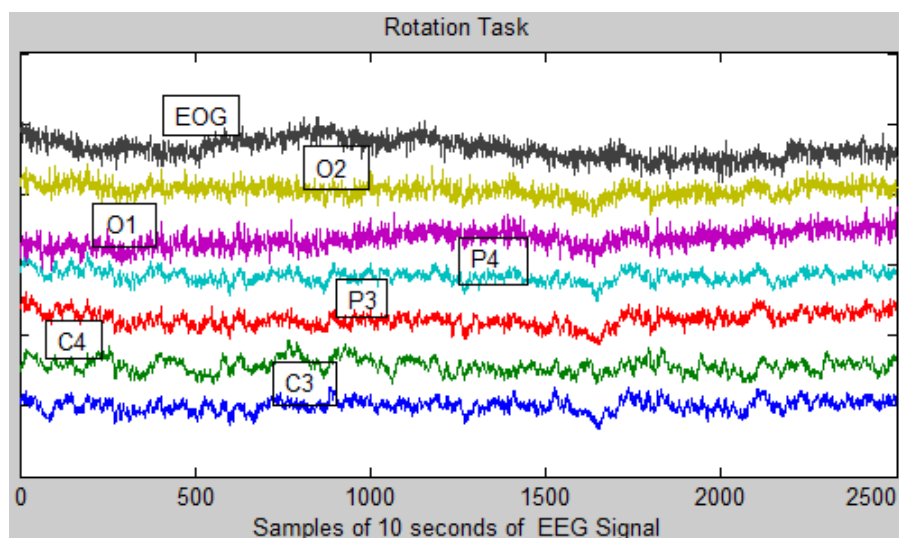


Figure 4.4–EEG Signals Recording of 7 Electrodes

In Figure 4.4, EEG signal voltage varied in between -50 to 50 microvolts and recording of signals corresponding to rotation task from 7 electrodes are shown. Signals were amplified using a bank of Grass 7P511 amplifiers and passed through a band pass filter with frequencies set to 0.1 to 100Hz. Signals were digitized through Lab Master A/D converter mounted in an IBM-AT computer using 12 quantization bits at 250Hz sampling frequency.

Subject 1, Subject 3, Subject 4 and Subject 6 completed 10 trials for each mental task. These trials were conducted on two days. Subject 2 and Subject 7 only completed 5 trials while Subject 5 completed 15 trials for each mental task. Therefore total trials were 325 with 65 trials for each mental task was performed. Each trial was of 10 seconds duration hence $250 \times 10 = 2500$ samples were recorded

4.3 Pre-Processing

The purpose of pre-processing block is to bring signals into a suitable form for feature extraction by removing to the extent possible variations (noise, artifacts etc.) that introduces randomness to the signal.

4.3.1 Colorado University Dataset

Each trial in the dataset was initially non-linearly normalized to reduce the range of EEG signals between 0 and 1 and each trial was segmented into windows of 1sec with an overlap of 0.5sec to reduce the execution time and memory utilization in processing 10 seconds of EEG signal [2],[3]. Normalized and segmented data was divided into training and testing data with 40 – 60 ratios respectively for client data. Since there was an overlap of 0.5sec in segmented data, it was ensured that there were no overlapping windows between training and testing data to maintain cross-validation. Subj. 1, Subj. 3, Subj. 4, and Subj. 6 were alternatively treated as clients. Since training based on multiple days improves overall system performance [19], equal no. of trials for both days were distributed for training and testing data except for Subj. 2, Subj. 5 and Subj. 7. Trials of Subj. 2, Subj.7, Subj. 5 and all subjects other than the client were used as imposter data.

4.3.2 Self-Recorded Dataset– I and II

Analog Input object in Mathworks Matlab® software was used to read composite EEG signal from the soundcard. The sound card was configured to operate in mono mode and sampling frequency was adjusted to 44100 samples/sec. Samples per trigger was adjusted to 44100 to read data from the soundcard in blocks of 1sec duration. Matlab® Filter toolbox was used to design FIR Least Square band pass filters with stop band attenuation of 60dB. Envelope detection method was used to demodulate the Amplitude modulated signal. Demodulated signal was down sampled to 1050Hz and was passed through low-pass filter with cutoff frequency 49Hz.

The demodulated filtered data of Dataset–I was stored in a 1x720 cell structure containing data of 4 subjects for two days. Each cell contained subject identification, task performed, trial number, demodulated signals of four channels, composite signal, session number and day number. The demodulated filtered data of Dataset–II was stored in an 11x80 cell structure containing data of 11 subjects. Each row contained data from single subject.

Figure 4.5 shows the demodulated signals recorded from Four Channel EEG machine.

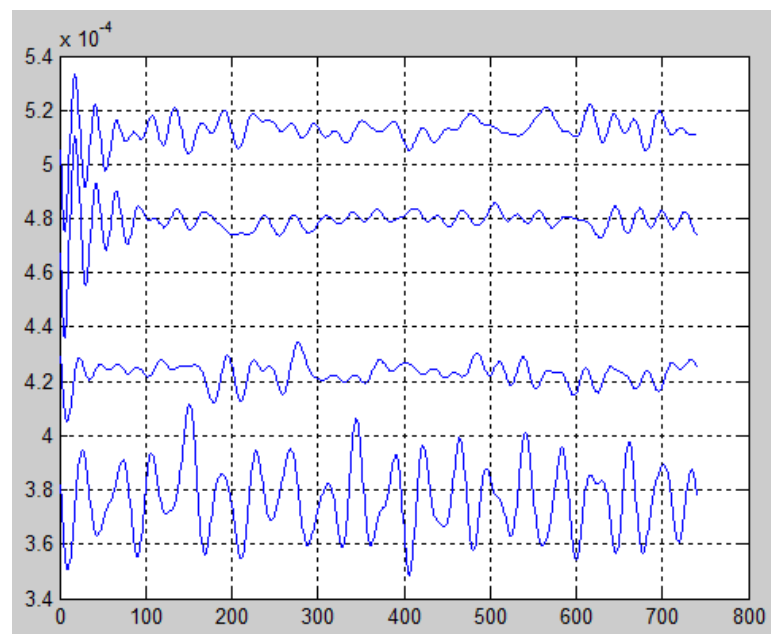


Figure 4.5–Demodulated Four Channel EEG Data

In Figure 4.5, x-axis shows the number of signal samples and y-axis shows the amplitude. A comparison of these signals with available EEG machines was beyond

the scope of this study. Although at the time of initial prototype design an effort was made to carry out a comparison of demodulated signals with a commercial EEG machine from Nihon Kohden® but the efforts proved unsuccessful as recorded signals decoding failed due to proprietary software.

4.4 Feature Extraction

Fractional spectral coefficients values were extracted for each one second of segmented EEG data using Fractional Fourier Transform (FRFT). The value of the order ‘a’ was optimized during validation for each electrode, task and subject using slightly modified coarse to fine approach proposed by [26]. The optimum order was selected which maximizes the classifier performance. The steps involved in the order optimization are listed in Figure 4.6, where λ and ϵ are positive numbers less than 1.

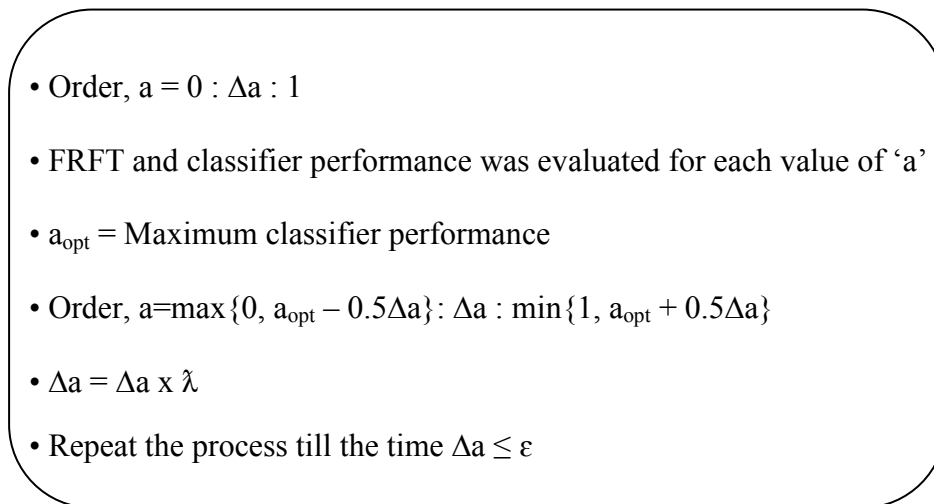
- 
- Order, $a = 0 : \Delta a : 1$
 - FRFT and classifier performance was evaluated for each value of ‘a’
 - a_{opt} = Maximum classifier performance
 - Order, $a = \max\{0, a_{opt} - 0.5\Delta a\} : \Delta a : \min\{1, a_{opt} + 0.5\Delta a\}$
 - $\Delta a = \Delta a \times \lambda$
 - Repeat the process till the time $\Delta a \leq \epsilon$

Figure 4.6–Order Optimization

4.5 Classification

Features extracted from each electrode channel were passed to Exact Radial Basis (RBE) Neural Network. The output of each neural network corresponding to the electrode was independent. RBE was selected as a classifier due to its low training time. It consists of one hidden radial basis layer containing as many neurons as input vectors and an output linear layer. One bit target vector was selected assigning a high value for the client and a low value for the imposter.

RBE neural network calculates the distance between incoming signal vector and its weight vector adjusted during training resulting in an output of radial basis neuron greater than 0.5 if the distance is less than spread chosen. Spread determines the distance an input vector must be from a neuron's weight vector for the output to be equal to 0.5.

A threshold was calculated for individual neural network classifier using a special one dimensional case of k-means clustering. Initial threshold was assumed to be 0.5. Response of Neural Network Classifier was distributed in two portions based on the initial threshold. Means of both the portions were calculated and their average was taken as the new threshold. This process was iteratively repeated till the time the difference of two consecutive thresholds was either zero or less than pre-decided small number. Radial Basis Function response for spread = 1 is shown in Figure 4.7.

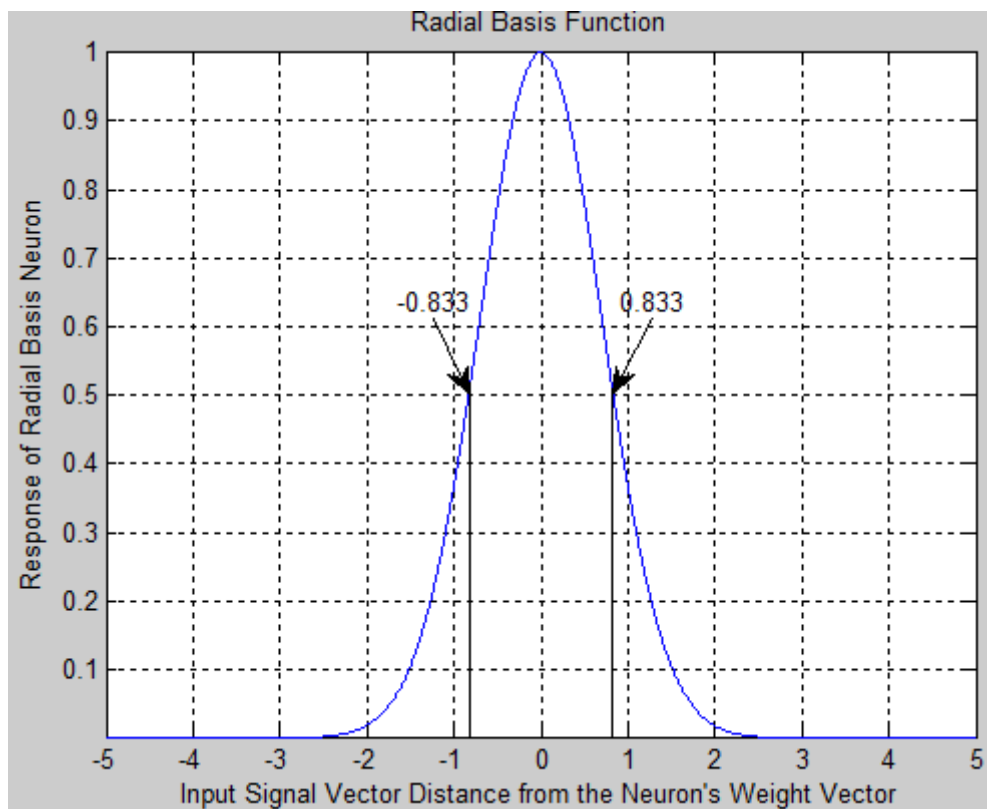


Figure 4.7–Radial Basis Function Response for Spread = 1

As evident from Figure 4.7, if the distance between input's signal vector and neuron's weight vector is $|0.833|$ then the response of Radial basis neuron will be equal to 0.5.

4.6 Network Weight Adjustment

Consider $X = \{E_1, E_2, E_3 \dots E_N\}$ represents N independent electrode channels in a BCI system and $Y = \{P(E_1), P(E_2), P(E_3), \dots, P(E_N)\}$ represents probability of correct classification for respective channels.

4.6.1 Simple Majority Rule

In simple majority rule the fundamental assumption is $P(E_1) = P(E_2) = \dots = P(E_N) = P$ as such decision of each electrode channel comprising the panel is equally weighted. If the number of electrodes (\hat{r}) that makes a correct classification decision is a binomial random variable (N, P) then probability that the panel comprising N electrodes makes a correct decision is given by:

$$P(\hat{r} \geq l) = \sum_{i=l}^N \binom{N}{i} (P)^i (Q)^{N-i} \quad \dots (4.1)$$

where $l = \left\lceil \frac{2N+1}{4} \right\rceil$, $\lceil \rceil$ represents ceiling function. l is the minimum number of independent electrode channels reaching a correct decision whose combined output results in the entire panel's decision to be correct and $Q = 1 - P$ represents the probability that an electrode channel makes a wrong classification decision. As mentioned earlier, the ability of the feature extractor algorithm to extract features from signals corresponding to different brain locations is not uniform hence classification accuracy also varies from one electrode to another. Classification based on simple majority rule does not take into account this phenomena resulting in erroneous or suboptimal classification.

4.6.2 Weight Adjustment

If $P(E_1) \neq P(E_2) \neq \dots \neq P(E_N)$ and the probability that all N electrodes comprising the panel makes a correct classification is given by:

$$P(E_N) = \prod_{j=1}^N P(E_j) \quad \dots (4.2)$$

Then the probability that panel makes correct classification decision is equal to the individual sum of probabilities of $\{E_N, E_{N-1}, E_{N-2}, \dots, E_l\}$ channels making a correct classification decision and is given by:

$$P'(\hat{r} \geq l) = \left\{ \begin{array}{l} P(E_N) + \sum_{i=1}^N Q(E_i) \left[\prod_{j=1}^N P(E_j) \right]_{j \neq i} + \\ \sum_{u=1}^N Q(E_u) \left[\sum_{i=u+1}^N Q(E_i) \left[\prod_{j=1}^N P(E_j) \right]_{\substack{j \neq u \\ j \neq i \\ u < N \\ i \neq u}} \right] + \dots \\ \dots + P(E_l) \end{array} \right. \quad \dots (4.3)$$

In case of $N=6$ electrode channels the above equation is reduced to:

$$P'(\hat{r} \geq 4) = \left\{ \begin{array}{l} \prod_{j=1}^6 P(E_j) + \sum_{i=1}^6 Q(E_i) \left[\prod_{j=1}^6 P(E_j) \right]_{j \neq i} + \\ \sum_{u=1}^6 Q(E_u) \left[\sum_{i=u+1}^6 Q(E_i) \left[\prod_{j=1}^6 P(E_j) \right]_{\substack{j \neq u \\ j \neq i \\ u < 6 \\ i \neq u}} \right] \end{array} \right. \quad \dots (4.4)$$

In order to apply weight adjustment, individual weights for each electrode are calculated using the equation:

$$W(E_s) = \frac{P(E_s)}{\Psi} * 100 \quad \dots (4.5)$$

where $\Psi = \sum_{j=1}^N P(E_j) \neq 1$ is sum of probabilities of the individual channels, N is the total number of channels in the system and $W(E_s)$ represent the weight of E_s electrode network. The probability of the Electrodes panel making correct classification after weight adjustment becomes:

$$P''(\tau \geq (l-1)) = P'(\hat{r} \geq l) + \left[\sum_{i_k=1}^N (Q(E_{i_k}) * \mathbb{Z}) \right]_{\sum W(E_s) > 50} \quad \dots (4.6)$$

where $k = N - l + 1$ and

$$\mathbb{Z} = \left[\sum_{i_{k-1}=i_k+1}^N Q(E_{i_{k-1}}) \dots [\mathbb{M}]_{i_3 < N-1} \right]_{i_k \leq k+1}$$

And

$$\mathbb{M} = \sum_{i_2=i_3+1}^N Q(E_{i_2}) [\mathbb{Y}]_{i_2 < N} ,$$

And

$$\mathbb{Y} = \left[\sum_{i_1=i_2+1}^N Q(E_{i_1}) \left[\prod_{j=1}^N P(E_j) \right]_{\substack{j \neq i_k \\ \vdots \\ j \neq i_2 \\ j \neq i_1}} \right]$$

Here l is the same as defined in Eq. (4.1) and Q_k is the probability that k^{th} electrode makes a wrong decision. Eq. (4.5) represents sum of probabilities that $(l-1)$ or more electrodes make a correct decision. The second term in Eq. (4.6) has the condition that sum of the individual weights of all possible combinations of $(l-1)$ electrodes reaching a correct decision is greater than 50. In case of $N=6$ electrode channels the above equation is reduced to:

$$P''(\tau \geq 3) = P'(\hat{r} \geq 4) + \left[\sum_{i_3=1}^6 (Q(E_{i_3}) \left[\sum_{i_2=i_3+1}^6 Q(E_{i_2}) [\mathbb{Y}]_{i_2 < 6} \right]_{i_3 < 5} \right]_{\sum W(E_s) > 50} \dots (4.7)$$

Where

$$\mathbb{Y} = \sum_{i_1=i_2+1}^6 Q(E_{i_1}) \left[\prod_{j=1}^6 P(E_j) \right]_{\substack{j \neq i_k \\ \vdots \\ j \neq i_2 \\ j \neq i_1}}$$

4.7 Performance Evaluation

In an authentication system there are two types of errors that can occur.

False Acceptance Rate (FAR): It is a type – II error that is system makes an incorrect decision and gives access to an imposter and is typically calculated as the ratio of number of false acceptances to number of access attempts.

False Rejection Rate (FRR): It is a likelihood measure that a valid client is denied access to the system and is usually calculated as a ratio of number of false rejections to number of authentication attempts.

The various models used for Authentication system attempts to reduce the above two errors. A unique measure known as Half Total Error Rate (HTER) is often used to evaluate the performance of authentication systems. HTER combines the above two ratios and is given as:

$$HTER = \frac{FAR + FRR}{2} \quad \dots (4.8)$$

4.8 Summary

To summarize captured EEG signals of all the electrodes are first log normalized and are transformed to the optimum fractional order. The fractional coefficients obtained are passed through a parallel neural network structure and its corresponding output is compared with the threshold computed during validation using one dimensional k-means clustering and interim response of each electrode in the panel is obtained. The cumulative sum of weighted individual response of each electrode is used for final classification decision to either deny or grant access to the user.

RESULTS AND ANALYSIS

5.1 Introduction

In this chapter, the algorithm is systematically tested on pre-recorded datasets to test the efficiency of the algorithm design. The emphasis of the tests performed was to analyze the performance of the classifier for various mental and motor imagery tasks and to determine the variation in individual electrode characteristics, corresponding weights and optimized order that results from one subject to another.

5.2 Offline Pre-Recorded Dataset Results

The \overline{HTER} performance of the authentication system for Subject 1 is shown in Figure 5.1. The figure contains the results of authentication for all the mental imagery tasks for all the electrode networks. The average performance of the authentication system for all the electrodes and mental imagery tasks for Subj. 1 was observed to be approximately 70%. E1, E2, E3 etc. are different electrode networks in Figure 5.1.

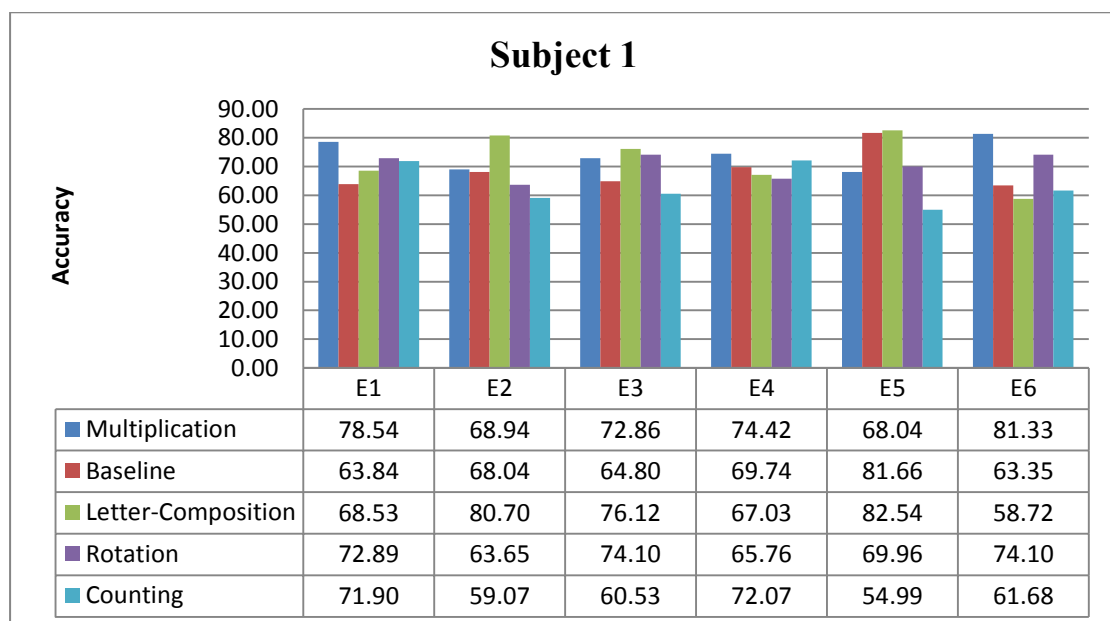


Figure 5.1–Individual Electrode \overline{HTER} Performance Curve for Subj. 1

The average performance of Subj. 3, Subj.4 and Subj. 6 for all the electrodes and mental imagery tasks was observed to be approximately 67%, 68% and 71% respectively as shown in Figures 5.2-5.4.

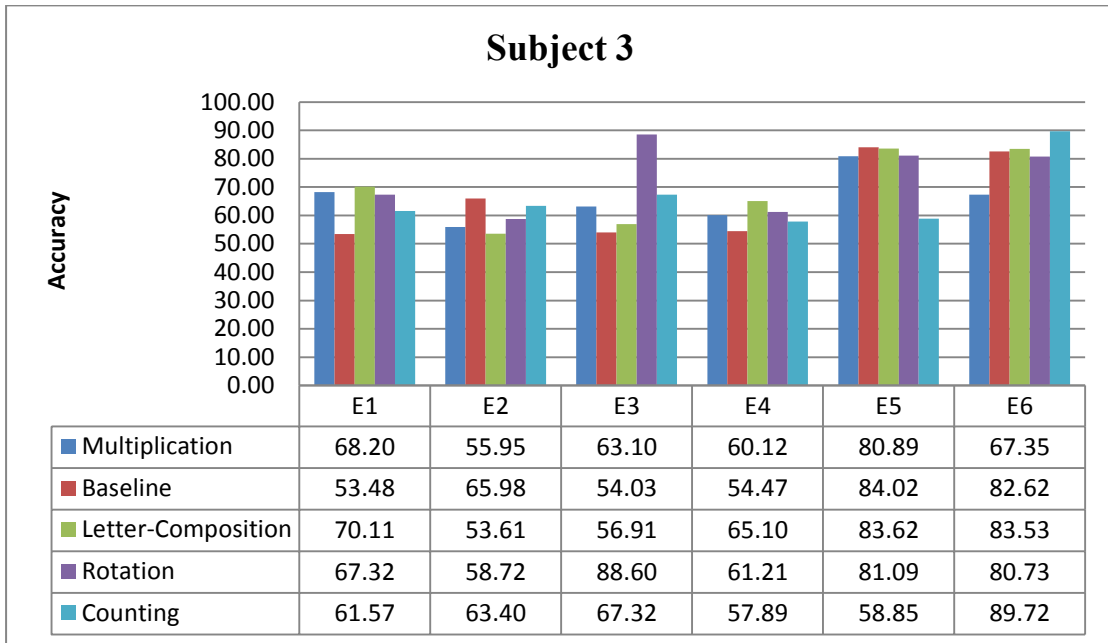


Figure 5.2–Individual Electrode \overline{HTER} Performance Curve for Subj. 3

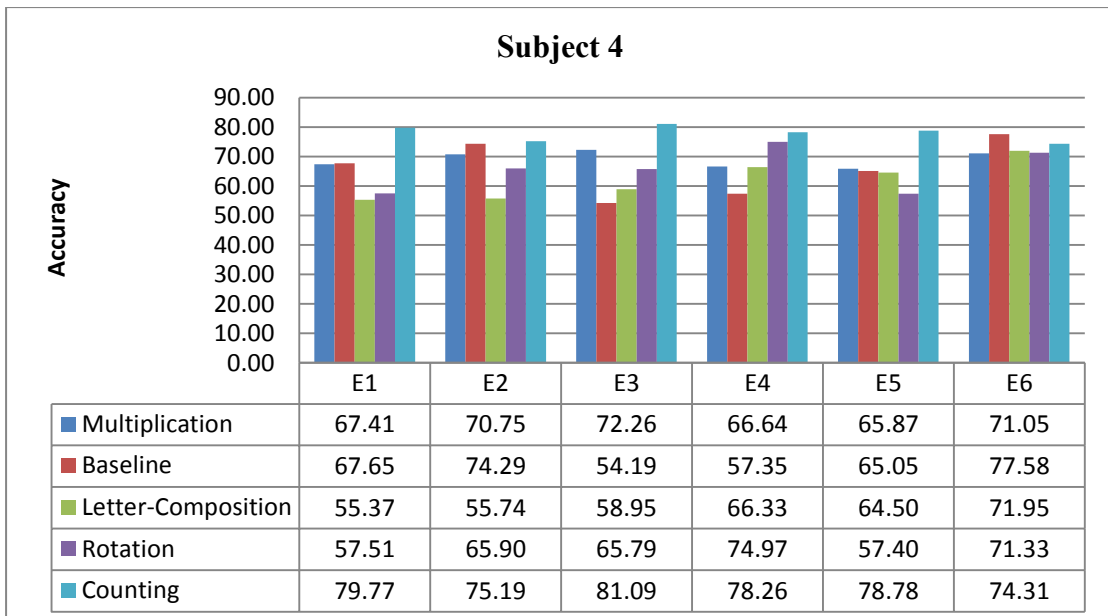


Figure 5.3–Individual Electrode \overline{HTER} Performance Curve for Subj. 4

Results shown in figures above indicate that the performance of classifiers not only vary from one subject to another but also for each electrode and task performed. Also for each user there is a different task that results in most efficient performance of the classifier which implies that weights adjustment to be carried out for one user might not necessarily be the same for another user. Depending upon the tasks being performed only those electrodes can be selected which provides higher performance for a particular subject. The efficiency of the classifier varies from one subject to another, hence a variable training time would also improve system performance i.e., users with low classifier response would require an increased amount of training time.

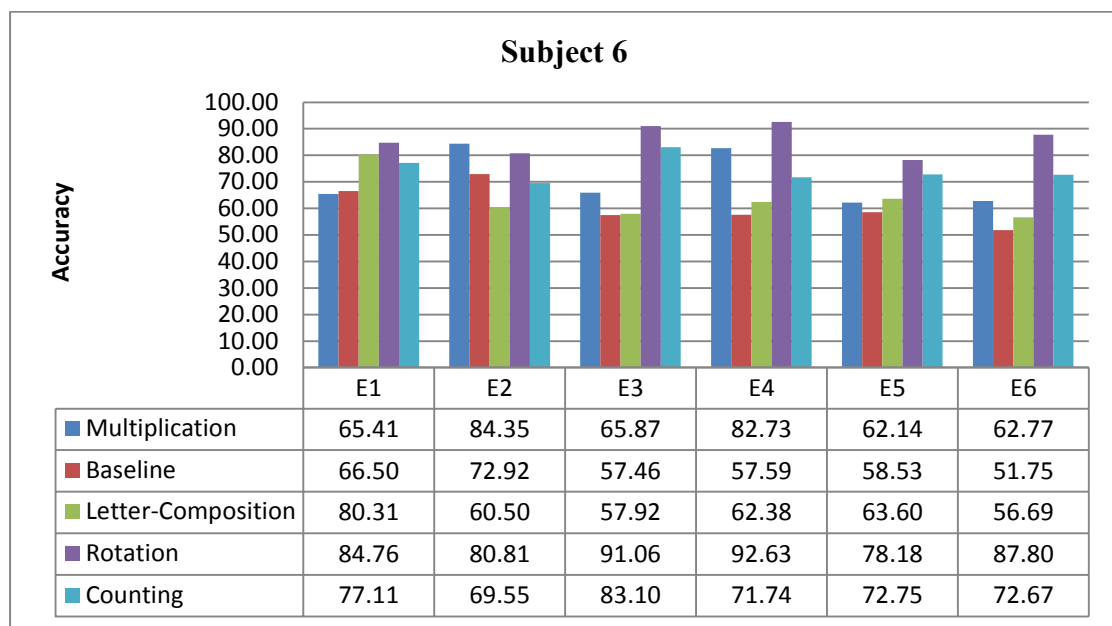


Figure 5.4–Individual Electrode \overline{HTER} Performance Curve for Subj. 6

Table 5.1–INDIVIDUAL ELECTRODE ACCURACIES FOR ALL MENTAL IMAGERY TASKS

Electrodes	Subj. 1	Subj. 3	Subj. 4	Subj. 6
E ₁	71.14	64.14	65.54	74.82
E ₂	68.08	59.53	68.37	73.62
E ₃	69.68	65.99	66.46	71.08
E ₄	69.81	59.76	68.71	73.41
E ₅	71.44	77.69	66.32	67.04
E ₆	67.83	80.79	73.24	66.34

The Table 5.1 lists average performance for all the mental imagery tasks for individual electrodes for all the subjects.

Table 5.2—OPTIMUM FRACTIONAL ORDERS FOR
MENTAL IMAGERY TASKS SUBJECT 1

Electrodes	Mental Imagery Tasks				
	Multiplication Task	Baseline Task	Letter Task	Rotation Task	Counting Task
E ₁	1	1	1	1	1
E ₂	0.9	1	1	0.7	0.9
E ₃	1	1	1	1	0.9
E ₄	1	1	0.5	1	1
E ₅	1	1	1	1	0.6
E ₆	0.9	1	0.1	1	1

Table 5.3—OPTIMUM FRACTIONAL ORDERS FOR
MENTAL IMAGERY TASKS SUBJECT 3

Electrodes	Mental Imagery Tasks				
	Multiplication Task	Baseline Task	Letter Task	Rotation Task	Counting Task
E ₁	1	1	1	0.9	0.8
E ₂	0	0.9	0.8	0.2	0
E ₃	0.9	0.7	0.9	1	1
E ₄	0.7	0.3	0	0.9	0.5
E ₅	1	1	1	1	1
E ₆	0.9	1	1	1	1

Table 5.4—OPTIMUM FRACTIONAL ORDERS FOR
MENTAL IMAGERY TASKS SUBJECT 4

Electrodes	Mental Imagery Tasks				
	Multiplication Task	Baseline Task	Letter Task	Rotation Task	Counting Task
E ₁	1	1	0.8	0	1
E ₂	1	1	0.8	1	0.9
E ₃	0.9	0.9	0.2	1	1
E ₄	0.9	1	1	1	1
E ₅	1	1	1	0.5	1
E ₆	0.9	1	1	1	1

Table 5.5—OPTIMUM FRACTIONAL ORDERS FOR
MENTAL IMAGERY TASKS SUBJECT 6

Electrodes	Mental Imagery Tasks				
	Multiplication Task	Baseline Task	Letter Task	Rotation Task	Counting Task
E ₁	0.9	0.9	1	1	1
E ₂	1	1	0.8	1	0.7
E ₃	0	0.7	0.7	1	1
E ₄	0.1	0.7	0.9	1	0.8
E ₅	1	1	1	1	1
E ₆	0.7	1	1	1	1

The Tables 5.2–5.5 list the optimum fractional orders for each subject, mental imagery tasks and electrodes. Fractional order not only varies from one subject to another but also from one task to another. The mental imagery task for which an order has been optimized will provide poor results for other mental imagery tasks, providing another layer of protection against imposters as not only the brain waves of the client have to be duplicated but also the mental imagery task for which the system was trained and optimized.

Table 5.6–WEIGHT ADJUSTMENT FOR MENTAL IMAGERY TASKS SUBJ. 1

Weights Adj.	Mental Imagery Tasks Subject 1				
	Mul.	Baseline	Letter.	Rotation	Count.
W(E ₁)	18	16	16	17	19
W(E ₂)	16	17	19	15	16
W(E ₃)	16	16	18	18	16
W(E ₄)	17	17	15	16	19
W(E ₅)	15	20	19	17	14
W(E ₆)	18	15	14	18	16

Table 5.7–WEIGHT ADJUSTMENT FOR MENTAL IMAGERY TASKS SUBJ. 3

Weights Adj.	Mental Imagery Tasks Subject 3				
	Mul.	Baseline	Letter.	Rotation	Count.
W(E ₁)	17	14	17	15	15
W(E ₂)	14	17	13	13	16
W(E ₃)	16	14	14	20	17
W(E ₄)	15	14	16	14	15
W(E ₅)	20	21	20	19	15
W(E ₆)	17	21	20	18	22

Table 5.8–WEIGHT ADJUSTMENT FOR MENTAL IMAGERY TASKS SUBJ. 4

Weights Adj.	Mental Imagery Tasks Subject 4				
	Mul.	Baseline	Letter.	Rotation	Count.
W(E ₁)	16	17	15	15	17
W(E ₂)	17	19	15	17	16
W(E ₃)	17	14	16	17	17
W(E ₄)	16	14	18	19	17
W(E ₅)	16	16	17	15	17
W(E ₆)	17	20	19	18	16

Table 5.9–WEIGHT ADJUSTMENT FOR MENTAL IMAGERY TASKS SUBJ. 6

Weights Adj.	Mental Imagery Tasks Subject 6				
	Mul.	Baseline	Letter.	Rotation	Count.
W(E ₁)	15	18	21	16	17
W(E ₂)	20	20	16	16	16
W(E ₃)	16	16	15	18	19
W(E ₄)	20	16	16	18	16
W(E ₅)	15	16	17	15	16
W(E ₆)	15	14	15	17	16

Tables 5.6–5.9 lists the weight adjustments for Subj. 1, Subj. 3, Subj. 4 and Subj. 6 calculated using Eq. 3 for the electrodes performance for various mental tasks shown in Figure 5.1–5.4 respectively. High fidelity electrodes are provided higher weights and these weights vary for different electrodes, subjects and from one mental task to another.

Table 5.10–EXPECTED SYSTEM PERFORMANCE FOR MENTAL IMAGERY TASKS

Tasks	Subject 1		Subject 3	
	Without W(E _s)	With W(E _s)	Without W(E _s)	With W(E _s)
Mult.	81.62%	90.65%	66.72%	82.97%
Baseline	71.87%	85.89%	66.61%	85.45%
Letter	78.91%	90.50%	72.73%	88.30%
Rotation	74.65%	85.76%	80.38%	92.64%
Counting	61.45%	77.71%	67.83%	86.93%
Average	73.7%	86.10%	70.85%	87.26%

Expected Authentication system accuracy based on individual electrode performances for all the tasks of Subject 1 and 3 with and without weight adjustment is shown in Table 5.10. The expected results were calculated using Eq.4.4 and 4.7. The weights are highly dependent on the validation data if the performance evaluated for the validation data does not represent the testing data, system performance will be degraded instead of improvement. Also weight adjustment will be ineffective for less than three channels as weight adjustment in such a scenario would simply cancel the response of the electrode with lower performance. Any channel having performance less than 50% will degrade the performance of the entire system. Figure 5.5 illustrates the weighted performance for all the tasks for various subjects. Average weighted performance of Subj. 1 equals to 81% and Subj. 3 equals to 84% which is an average improvement of approximately 14% over the system without any weight adjustment

while expected performance improvement was calculated to be 14.4%. The results shown indicates that system provides optimal performance for letter-composition task in case of Subject 1, rotation task in case of Subject 3 and Subject 4 and counting task in case of Subject 6. The results depicted in Figure 5.5 are for small training data (40%) and they can be further improved to nearly 100% by using groups of multiple consecutive segments and applying the voting rules for authentication [21]. This approach however delays the system response with the delay dependent on number of consecutive segments used and the duration of each segment.

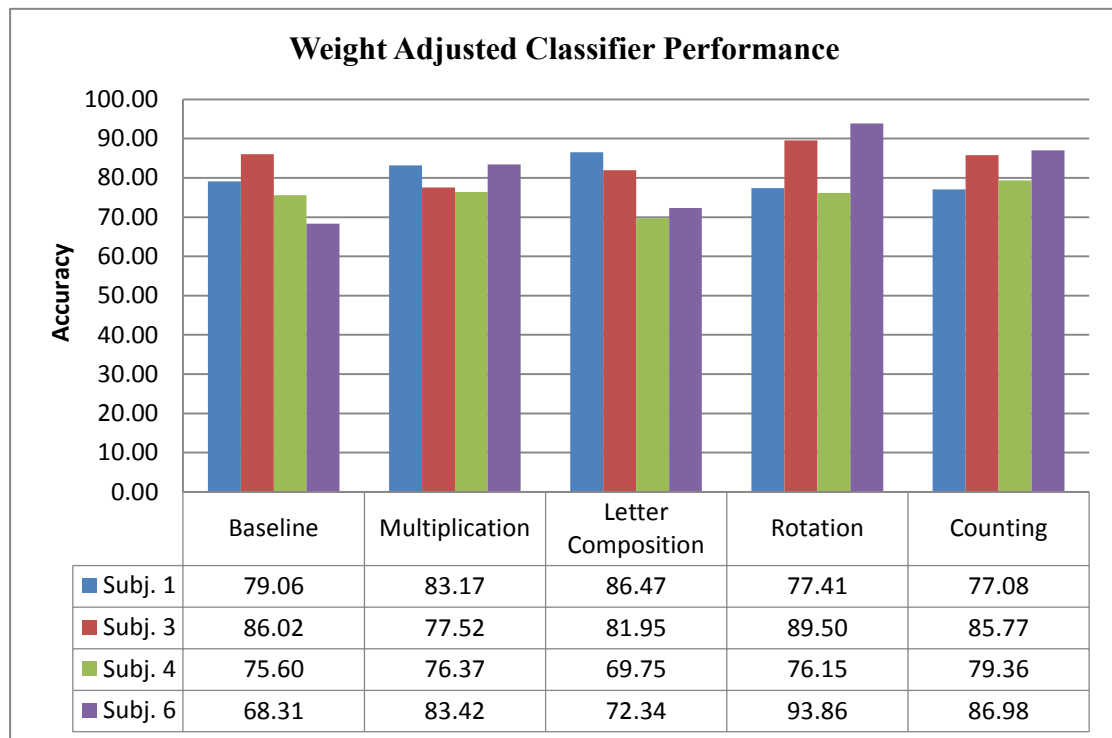


Figure 5.5–Weight Adjusted Performance for each Mental Imagery task for various Subjects

5.3 Offline Self-Recorded Dataset-I Results

The \overline{HTER} performance of the authentication system for Subject 2 and Subject 3 of self-recorded Dataset-I are shown in Figure 5.6 and Figure 5.7 respectively. The figures contains the results of authentication for all the mental imagery tasks for all the electrode networks. The average performance of the authentication system for all the electrodes and mental imagery tasks for Subj. 1 and Subj. 3 was observed to be approximately 56% and 57% respectively.

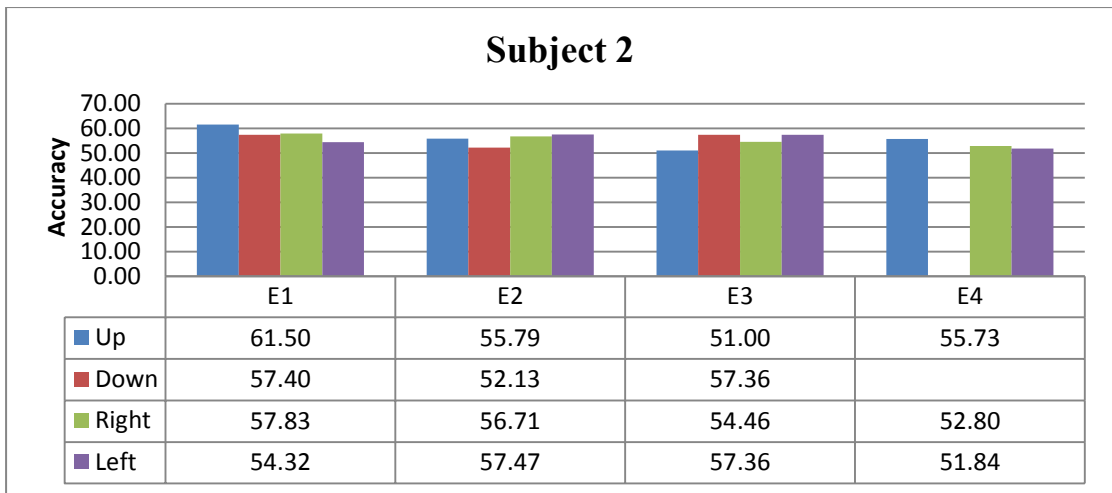


Figure 5.6–Individual Electrode Performance for Subj. 2

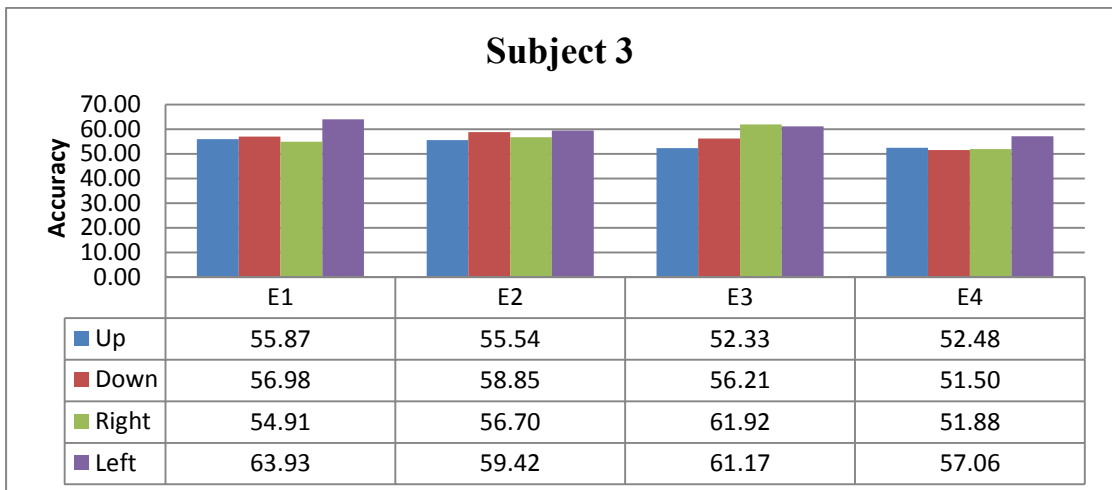


Figure 5.7–Individual Electrode Performance for Subj. 3

The results shown in Figure 5.6 and Figure 5.7 depict lower system performance compared to previous dataset. The reason for this lower response is the degraded and distorted signal recorded by signal acquisition device. The passive electrodes were used to record signals without any external shielding which resulted in a lot of noise being superimposed on the recorded signals. Secondly the human error involved in the placement of electrodes at almost the exact same location also resulted in increased false rejections therefore decreasing the overall \overline{HTER} performance. Performance of the system can be significantly improved if active electrodes with

proper insulation and an electrode cap for placement of electrodes is used during signal acquisition.

Table 5.11–INDIVIDUAL ELECTRODE ACCURACIES

Electrodes	Subj. 2	Subj. 3
E ₁	57.76	57.92
E ₂	55.52	57.63
E ₃	55.04	57.91
E ₄	53.46	53.23

Table 5.12–OPTIMUM FRACTIONAL ORDERS FOR MOTOR IMAGERY TASKS SUBJECT 2

Electrodes	Motor Imagery Tasks			
	Up Task	Down Task	Right Task	Left Task
E ₁	0.52	0.9	0.4	0.2
E ₂	0.8664	0.9	0	0.1
E ₃	0.17	0.9	1	0.2
E ₄	0.77	0.5	0.7	0.72

Table 5.13–OPTIMUM FRACTIONAL ORDERS FOR MOTOR IMAGERY TASKS SUBJECT 3

Electrodes	Motor Imagery Tasks			
	Up Task	Down Task	Right Task	Left Task
E ₁	0.4	0	0	0.8
E ₂	0.8	0.2	0	0.95
E ₃	0.5	0.8	1	0.99
E ₄	0.8	0.7	0.9	0.95

Table 5.14–WEIGHT ADJUSTMENT FOR MOTOR IMAGERY TASKS SUBJ. 2

Weights Adj.	Motor Imagery Tasks Subject 2			
	Up	Down	Right	Left
W(E ₁)	27	34	26	25
W(E ₂)	25	31	26	26
W(E ₃)	23	34	25	26
W(E ₄)	25	0	24	23

Table 5.15–WEIGHT ADJUSTMENT FOR MOTOR IMAGERY TASKS SUBJ. 3

Weights Adj.	Motor Imagery Tasks Subject 3			
	Up	Down	Right	Left
W(E ₁)	26	25	24	26
W(E ₂)	26	26	25	25
W(E ₃)	24	25	27	25
W(E ₄)	24	23	23	24

5.4 Offline Self-Recorded Dataset-II Results

The \overline{HTER} performance of the authentication system for Subject 1–11 of self-recorded Dataset-II are shown in Figures 5.8–5.18 respectively. The figures contain the results of authentication for all the mental imagery tasks for all the electrode networks. It could be seen from Table 5-16 that classifier offers consistently higher performance for all the subjects for signals recorded from Electrode-I except for Subject-9 for which Electrode - III results in highest efficiency.

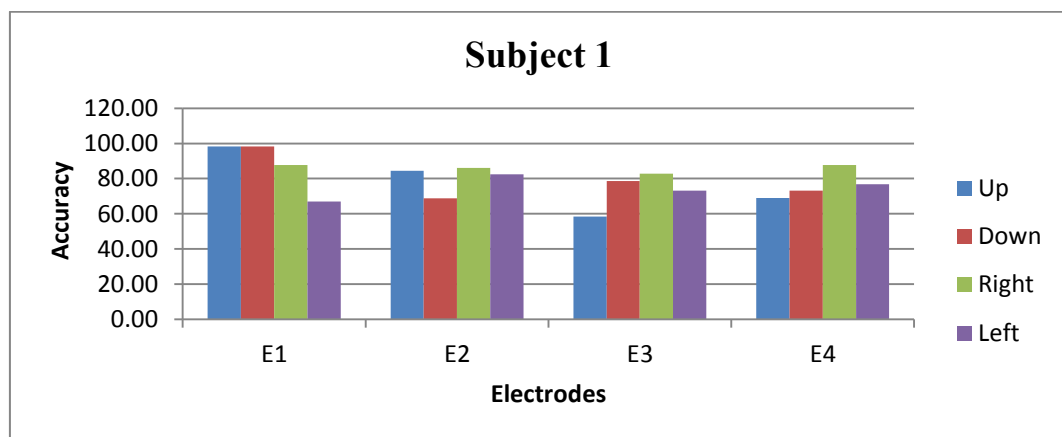


Figure 5.8–Individual Electrode Performance for Subj. 1 Dataset - II

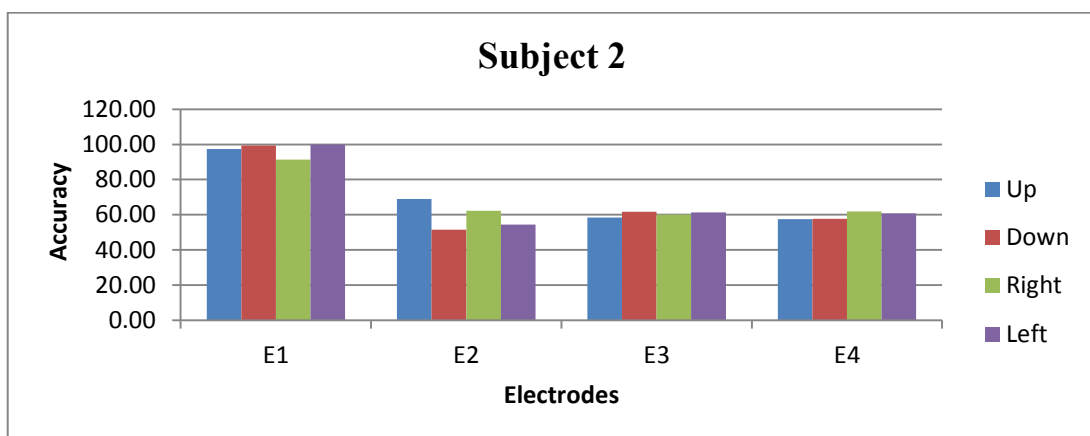


Figure 5.9–Individual Electrode Performance for Subj. 2 Dataset - II

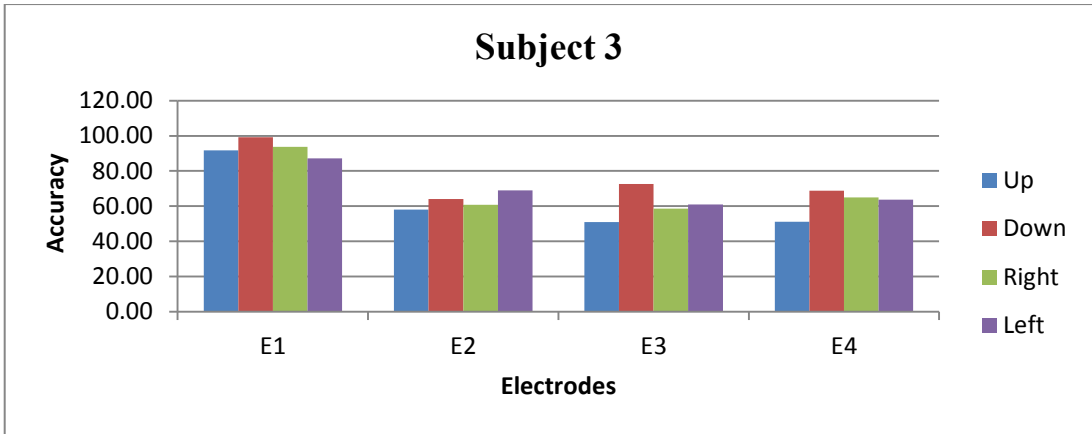


Figure 5.10–Individual Electrode Performance for Subj. 3 Dataset - II

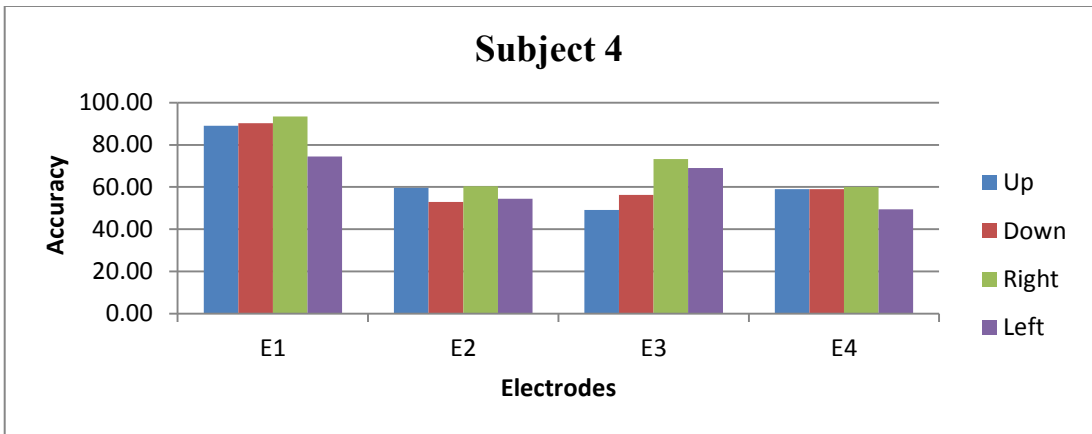


Figure 5.11–Individual Electrode Performance for Subj. 4 Dataset - II

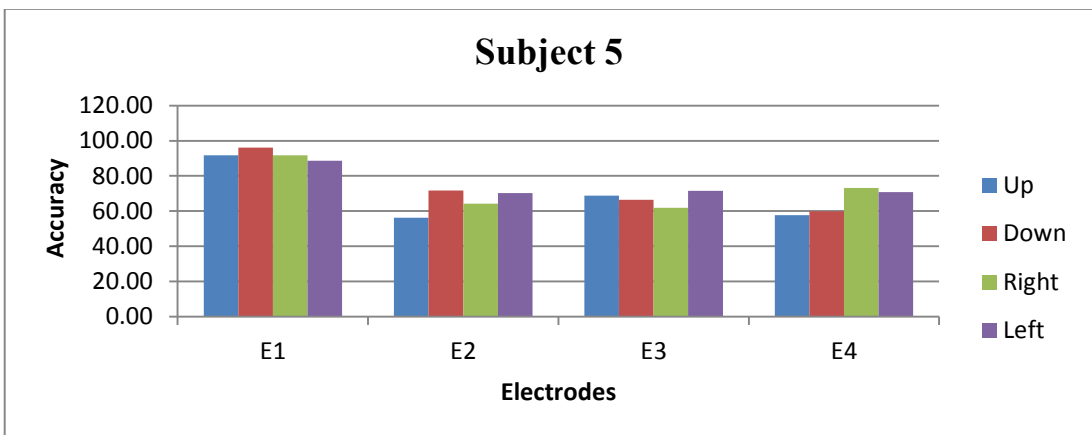


Figure 5.12–Individual Electrode Performance for Subj. 5 Dataset - II

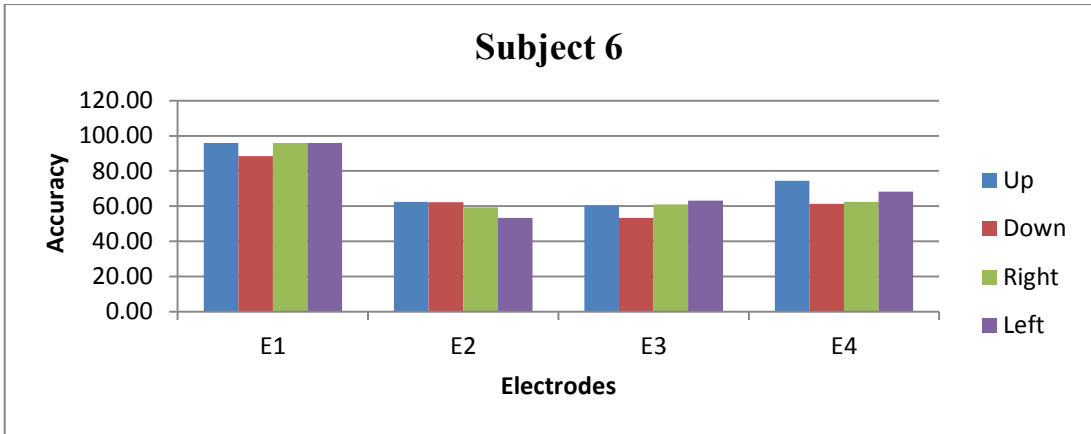


Figure 5.13–Individual Electrode Performance for Subj. 6 Dataset - II

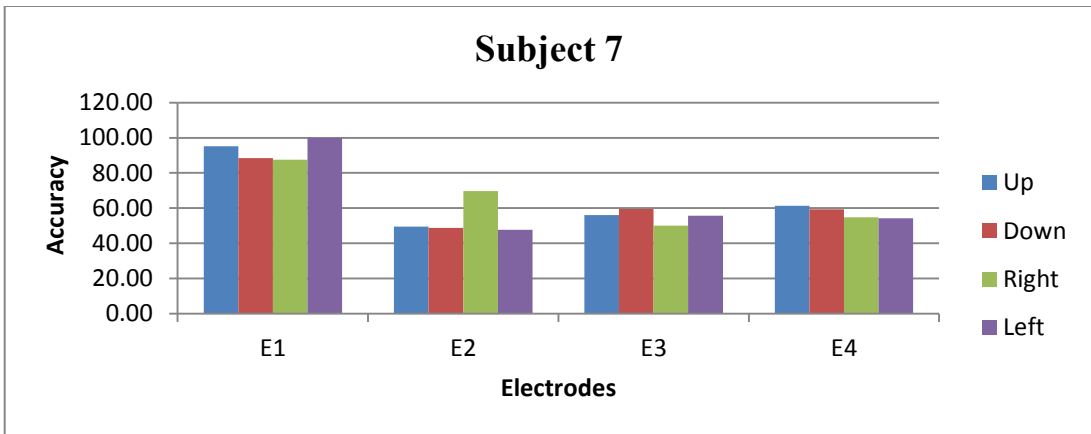


Figure 5.14–Individual Electrode Performance for Subj. 7 Dataset - II

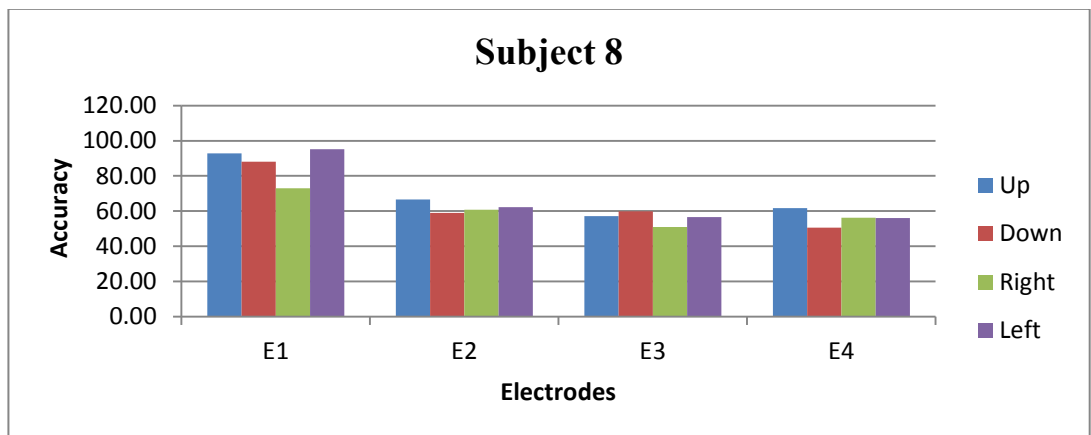


Figure 5.15–Individual Electrode Performance for Subj. 8 Dataset - II

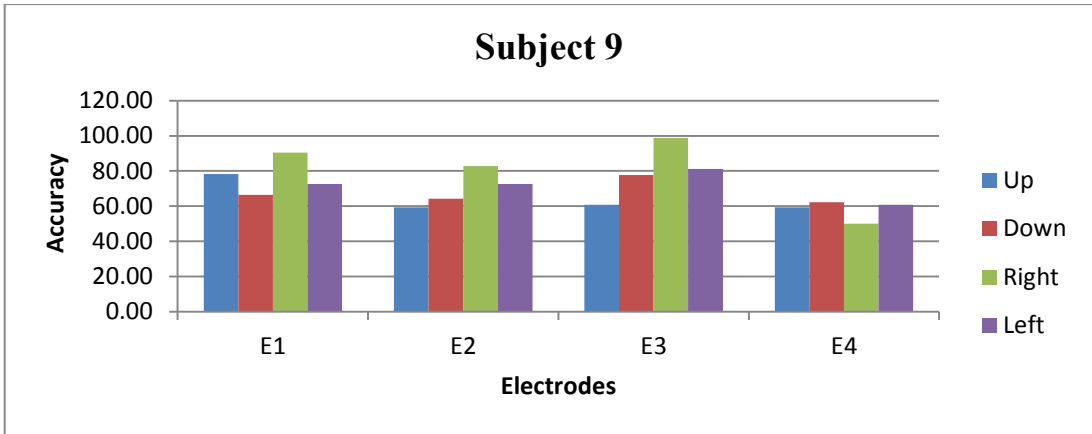


Figure 5.16–Individual Electrode Performance for Subj. 9 Dataset - II

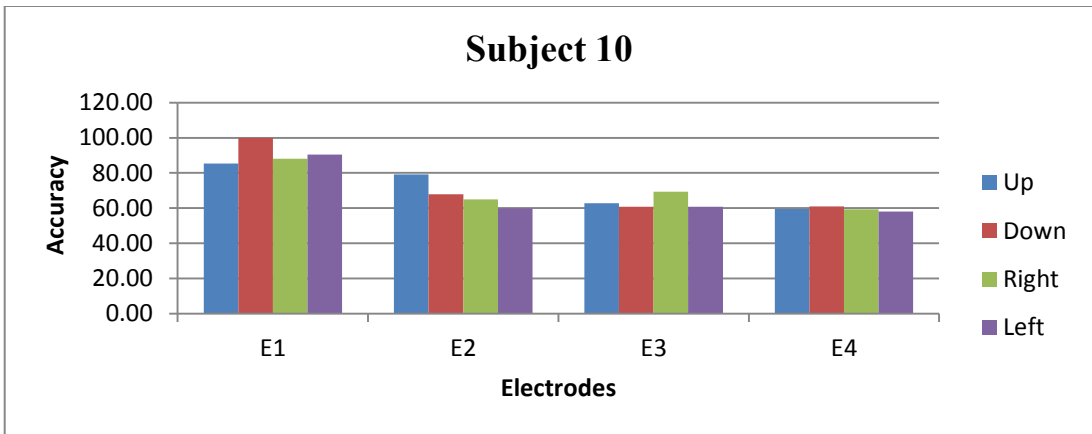


Figure 5.17–Individual Electrode Performance for Subj. 10 Dataset - II

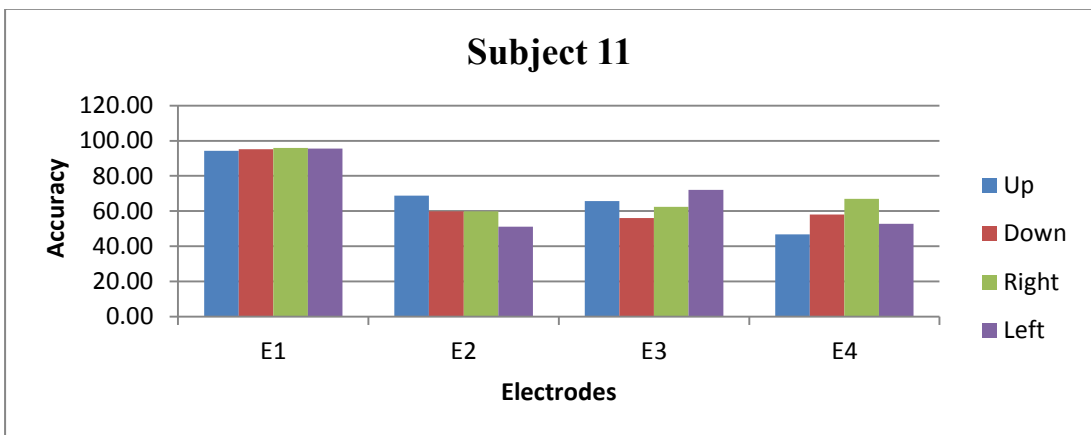


Figure 5.18–Individual Electrode Performance for Subj. 11 Dataset - II

Table 5.16—AVERAGE ELECTRODE ACCURACIES
FOR MOTOR IMAGERY TASKS FOR ALL SUBJECTS

SUBJECT	E1	E2	E3	E4
1	87.8	80.43	73.21	76.71
2	97.02	59.30	60.34	59.45
3	92.93	62.95	60.79	62.13
4	86.76	56.85	61.90	56.85
5	92.04	65.62	67.11	65.40
6	93.97	59.3	59.45	66.59
7	92.78	53.87	55.28	57.37
8	87.28	62.13	56.10	56.10
9	76.93	69.72	79.61	58.04
10	91	67.93	63.39	59.45
11	95.24	59.90	64.06	56.10

The results of Dataset–II are comparatively better than Dataset–I due to the fact that signal recordings were made only in a single session. Performance degradation over time cannot be gauged from single day recordings. The results provided in this chapter highlights the potential of a system based on Fractional Fourier Transform by offering better performance and flexibility of transform order to adjust system performance in varying conditions without altering the overall system design. The system results shown above are for a maximum response time of two seconds only. If a tradeoff is made between response time and system efficiency and several consecutive segments are used to authenticate a user the system response can be improved significantly.

5.5 Comparison Existing Techniques

The effective comparison of proposed algorithm with existing techniques requires that tests are carried out under similar conditions. Different approaches have been used on different datasets under different conditions and each leading to satisfactory performance. For instance, the pre-recorded dataset used in this work was also used by R. Palaniappan [31] for person identification using Autoregressive (AR) coefficients extracted through Burg's method with order six as features and Linear Discriminant Classifier was used for classification. The 50% of the entire data was used for training as opposed to 40% training data for clients used in this study. The average results obtained in [31] were around 95% and they were further improved by using two tasks in conjunction for the purpose of person identification. Although the response time for the offline analysis was similar to the one used in this study but if analyzed for online analysis the overall response time would be greater since the authentication system is a type of asynchronous BCI as such the user has to be provided sufficient time break between execution of two tasks resulting in overall slower response time.

Poulos et. al. [30] used spectral values extracted from EEG signals in overlapping alpha rhythm frequency bands 7-10Hz, 8-11Hz and 9-12Hz as features to identify users. The study was aimed at pointing out differences in classifier performance for different frequency bands for the single channel captured EEG signals. The dataset used comprised of multiple recordings from four clients and single recording each from 75 subjects were used for impersonation. No significant changes were observed and classification accuracy varied in between 72 – 84%.

In another approach the ratio of Power Spectral Density and Energy of the signal for each electrode is used to obtain normalized feature value for N number of electrodes and are concatenated together to form a feature vector. The drawback with this approach is large number of electrodes required to form a feature vector that results in reasonable classifier accuracy. To the best of author's knowledge weight adjustment based on electrode characteristics has never been carried out.

5.6 Summary

In this chapter, tests were carried out using proposed algorithm on datasets obtained from Colorado University and signals captured through indigenously prepared EEG machine. The experimental and mathematical results obtained suggest an average improvement of 10% in classifier performance for a weight adjusted response.

CONCLUSION AND FUTURE WORK

6.1 Overview

The Brain Computer Interface is currently a hot area of research. Existing BCI systems can be utilized for biometric systems in a multimodal environment that is a system utilizing more than one biometric parameter like Iris scan and Finger-printing utilized in unison to authenticate or identify a particular individual. At the same time Fractional Fourier Transform offers improved system performance and is a better feature extractor and analysis tool for time varying signals like EEG as compared to conventional Fourier Transform based techniques.

6.2 Objectives Achieved

The Fractional Fourier Transform is a relatively new signal processing tool. The work carried out in this research systematically analyzes the utilization of Fractional Fourier Transform and demonstrates its efficacy not only for EEG based person authentication but also for filtering noisy signals henceforth were impossible to filter. The examples simulated demonstrate how chirp signals can be detected and its parameters can be accurately estimated even in the presence of noise using FRFT. The order optimization was also achieved using the MACF algorithm resulting in faster system response. The weight adjustment method was used not only to predict the performance of the system but a variable training session was suggested to significantly improve individual user performance.

6.3 Future Work

Although a framework for the application of FRFT to Biometric systems is proposed but still a lot of problems exist that needs to be solved before the system can be successfully utilized. One of the problems include the dimensional normalization which is not considered in the present algorithm as DZPM causes such an increase in computational load making it impossible to be used in online situations. While DSM

method on the other hand only operates on time axis and its application is meaningless since neural networks only operate on signal amplitudes.

Influence of the user's physical and physiological conditions on the EEG signals was not part of this study. Subsequently the variations in EEG signal characteristics due to user's mental state needs to be monitored over large period of time and it remains to be seen whether these variations can be predicted and removed to effectively utilize EEG signals as a biometric tool.

Another question that still needs to be answered is the change in Fractional Order for a particular subject over time. It remains to be studied whether the change can be calculated and predicted and thereby incorporating it in the algorithm design to improve its performance. Also the use of Neuro-Fuzzy networks instead of neural networks might also improve system performance as it involves a true value that ranges in degrees between 0 and 1 instead of the binary output in case of RBE neural networks. Also the weight adjustment proposed and analyzed in this study can be extended to multiple feature extractors used in parallel for similar inputs to further improve classifier performance.

6.4 Summary

In this chapter various objectives achieved in the research work are summarized and some of the questions still left unanswered and suggestions based on observations made during experimentation for additional system improvements are listed as a potential area for further research in future.

BIBLIOGRAPHY

- [1] R. Scherer, F. Lee, A.Schlögl, R.Leeb, H.Bischof, and G. Pfurtscheller, “Toward Self-Paced Brain–Computer Communication: Navigation Through Virtual Worlds”IEEE Trans. On Biomedical Engg., Vol. 55 Issue 2, pp. 675-682, Date Feb. 2008
- [2] K. Nakayama, Y. Kaneda and A. Hirano, “A Brain Computer Interface based on FFT and Multilayer Neural Network-Feature Extraction and Generalization,” in Proc. International Symposium on Intelligent Signal Processing and Communication Systems (ISPACS) 2007, p. 826-829, Date. Nov.28-Dec.1, 2007
- [3] K. Nakayama and K. Inagaki, “A Brain Computer Interface Based on Neural Network with Efficient Pre-Processing,” in Proc. International Symposium on Intelligent Signal Processing and Communication Systems (ISPACS), 2006, p. 673-676, Date12-15 Dec. 2006
- [4] M.B. Khalid, N.I. Rao, I. Rizwan-i-Haque, S. Munir, and F. Tahir, “A Brain Computer Interface (BCI) using Fractional Fourier Transform with Time Domain Normalization and Heuristic Weight Adjustment,” 9th International Conference on Signal Processing, (ICSP) 2008, IEEE, pp. 2734 - 2737, Date. 26-29 Oct. 2008
- [5] R. N. Bracewell, “The Fourier Transform and its Applications,” ISBN:9780071160438, 3rd Edition McGRAW-HILL, 1999
- [6] B.Santhanam and T. S. Santhanam “On Discrete Gauss Hermite Functions and Eigenvectors of the Discrete Fourier Transform,” Signal Processing, Vol. 88 Issue 11, Elsevier, pp.2738-2746, Date Nov. 2008
- [7] M. Martone, “A Multicarrier System Based on the Fractional Fourier Transform for Time–Frequency-Selective Channels,” IEEE Transactions on Communications , Vol. 49 No. 6, pp. 1011-1020, Date Jun. 2001
- [8] H. Sun, F. Su, W. Wang and S. Tang, “Parameter Estimation of Moving Targets in Airborne SAR Based on Fractional Fourier Transform,” in Proc.

Microwave and Millimeter Wave Technology, ICMMT '07, p. 1-4, Date 18-21 Apr. 2007

- [9] H. M. Ozaktas and O. Arikan, "Digital computation of the fractional Fourier transform," IEEE Trans. On Signal Proc., Vol. 44, No. 9, pp.2141-2150, Date Sep. 1996.
- [10] B. Santhanam and J. H. McClellan, "The DRFT—A rotation in time frequency space," in Proc. on Acoustics, Speech, and Signal Processing (ICASSP), pp. 921–924. Date May 1995
- [11] S. C. Pei, C. C. Tseng, M. H. Yeh, and J. J. Shyu, "Discrete fractional Hartley and Fourier transform," IEEE Trans. Circuits System II, Vol. 45, No. 6, pp. 665–675, Date Jun. 1998
- [12] S. C. Bradford V, "Time-Frequency Analysis methods, including the Wigner-Ville Distribution: Applications to Transient Signals," <http://case.caltech.edu/tfr/>, 2012
- [13] R. Scherer, F. Lee, A. Schlogl, R. Leeb, H. Bischof, and G. Pfurtscheller, "Toward Self-Paced Brain-Computer Communication: Navigation Through Virtual Worlds," Transactions on Biomedical Engineering, Vol. 55, No. 2, IEEE, pp. 675-682, Date. Feb. 2008
- [14] J.S. Lin, K.C. Chen, and W.C. Yang, "EEG and eye-blinking signals through a Brain-Computer Interface based control for electric wheelchairs with wireless scheme," 2010 4th International Conference on New Trends in Information Science and Service Science (NISS), , IEEE, Korea (South), pp. 731-734, Date. 11-13 May 2010
- [15] B. Chambayil, R. Singla, and R. Jha, "Virtual keyboard BCI using Eye blinks in EEG," 2010 IEEE 6th International Conference on Wireless and Mobile Computing, Networking and Communications (WiMob), IEEE, Canada, pp. 466 - 470, Date.11-13 Oct. 2010
- [16] A. Amcalar, and M. Cetin, "A Brain Computer Interface System for Online Spelling," 2010 IEEE 18th Signal Processing and Communications

Applications Conference (SIU), IEEE, Turkey, pp. 196 - 199, Date.22-24 April. 2010

- [17] M. Poulos, M. Rangoussi, V. Chrissicopoulos, and A. Evangelou, "Person Identification Based on Parametric Processing on the EEG," Proc. Sixth Int'l Conf. Electronics, Circuits, and Systems (ICECS '99), vol. 1, pp. 283-286, Date 5-8 Sept. 1999
- [18] R. Palaniappan and K.V.R. Ravi, "A New Method to Identify Individuals Using Signals from the Brain," Proc. Fourth Int'l Conf. Information Comm. And Signal Processing, pp. 1442-1445, Date 15-18 Dec. 2003
- [19] S. Marcel, J. Del and R. Millan, "Person Authentication Using Brainwaves (EEG) and Maximum A Posteriori Model Adaptation," IEEE Trans. Pattern Analysis & Machine Intelligence Vol 29, No. 4, pp. 743-752, Date Apr. 2007.
- [20] B. Liu, J. Gao; Z. Liu; Z. Zhang; C. Yin, C. Peng and J. Gu, "Brainwave Classification Based on Wavelet Entropy and Event-Related Desynchronization" in Proc. Canadian Conference on Electrical and Computer Engineering (CCECE) , 2007, p. 1018-1021, Date 22-26 Apr 2007
- [21] T. N. Lal, M. Schroder, T. Hinterberger, J. Weston, M. Bogdan, N. Birbaumer and B. Scholkopf, "Support vector channel selection in BCI," IEEE Trans. On Biomedical Engineering, Vol.51, pp. 1003-1010, Date Jun. 2004
- [22] P. Tangkraingkij, C. Lursinsap, S. Sanguansintukul and T. Desudchit, "Selecting Relevant EEG Signal Locations for Personal Identification Problem Using ICA and Neural Network," in Proc.(ICIS), 2009, p. 616-621, Date 1-3 Jun. 2009
- [23] F. Oveisi, "Extracting components containing maximal information for EEG based-brain computer interface," in Proc. (NER'09), 2009, p. 319-322, Date 29 Apr. – 2 May 2009
- [24] H. M. Ozaktas, B. Barshan, L. Onural, "Filtering in fractional Fourier domains and their relation to chirp transforms," 7th Mediterranean Electro-technical Conference, 1994. Proceedings., p. 77 – 79 Vol. 1, Date 12-14 Apr. 1994

- [25] Z. Xinghao, T. Ran and D. Bing, "Practical Normalization methods in the Digital Computation of the Fractional Fourier Transform," Signal Processing, 2004. Proceedings.(ICSP'04), p.105-108 Vol. 1, Date 31 Aug. – 4 Sep. 2004
- [26] L. Zheng and D.Shee, "Maximum Amplitude Method for Estimating Compact Fractional Fourier Domain" IEEE Signal Processing Letters, Vol 17 No.3, pp. 293-296, Date Mar 2010
- [27] Y. Zhang, Q. Zhang, S. Wu, "Biomedical Signal Detection Based on Fractional Fourier Transform," IEEE Proceedings of the 5th International Conference on Information Technology and Application in Biomedicine, in conjunction with The 2nd International Symposium & Summer School on Biomedical and Health Engineering Shenzhen, China, p. 349-352, Date 30-31 May.2008
- [28] C.W. Anderson and M. Kirby, "Classification of Electroencephalogram (EEG) Signals for Brain-Machine Interfaces", <http://www.cs.colostate.edu/eeg>
- [29] Z. A. Keirn, "Alternative modes of communication between man and machine," Master's thesis, Purdue University, 1988
- [30] M. Poulos, M. Rangoussi and N.Alexandris, "Neural network based person identification using EEG features," in Proc. ICASSP, 1999, p.1117-1120 vol.2
- [31] R. Palaniappan, "Identifying Individuality Using Mental TaskBased Brain Computer Interface," in Proc. Of Intelligent Sensing and Information Processing, (ICISIP) 2005, p. 238-242, Date 14-17 Dec 2005